Characterisation of primary ciliary dyskinesia model generated from *BMI1* transduced basal epithelial cells

Melis T. Dalbay¹, Eriomina Shahaj¹, Ileana Guerrini¹, Dani Do Hyang Lee², Anna Straatman-Iwanowska⁴, Hannah M. Mitchison¹, Deborah L. Baines³, Robert A. Hirst⁴, Claire Hogg^{5,6}, Christopher O'Callaghan², Stephen L. Hart^{1,*}

ABSTRACT

Primary ciliary dyskinesia (PCD) is a rare genetic respiratory disorder, caused by a reduction in cilia number or dysmotility. Cilia dysmotility leads to breathing difficulties, concurrent infections and severe lung damage if not treated, with no therapies currently available. Improved airway epithelial cell models, that mimic the disease phenotype, are required for development of new therapeutics, as they exert limited potential of self-renewal *in vitro*. Here we describe a human PCD cell model by lentiviral transduction of airway basal epithelial cells with *BMI1* gene, a regulator of senescence. We report that the cells retain their proliferation and differentiation capacity for at least 19 passages and recapitulate the disease phenotype with immotile cilia lacking DNAH5 and other outer dynein arm proteins. Characterisation of the ion transport properties of these PCD cells grown at air-liquid interface showed lower activity of the sodium channel ENaC and enhanced CFTR activity compared to non-PCD cells, which may be linked to ciliary immotility. Our study provides a robust

¹Department of Genetics and Genomic Medicine, UCL Great Ormond Street Institute of Child Health, University College London, London WC1N 1EH, UK

²Department of Infection, Immunity & Inflammation, UCL Great Ormond Street Institute of Child Health, University College London, London, UK

³Institute for Infection and Immunity, St George's University, University of London, London, UK

⁴Centre for Primary Ciliary Dyskinesia Diagnosis and Research, Department of Respiratory Sciences, University of Leicester, Leicester, UK

⁵PCD Diagnostic Centre, Royal Brompton and Harefield NHS Trust, London SW3 6NP, UK

⁶Paediatric Respiratory Medicine, Imperial College London, London SW3 6NP, UK

^{*}Author for correspondence: S.hart@ucl.ac.uk

PCD model for therapeutic studies and may open new avenues to investigate the molecular mechanisms of this disease.

INTRODUCTION

Primary ciliary dyskinesia (PCD) is an autosomal recessive genetic disorder, estimated to affect in 1 in 10,000 live births, caused by variants in genes that encode for proteins governing multiciliogenesis program, leading to ciliary dysmotility (Legendre et al., 2021). Motile cilia are small hair-like organelles that protrude from the surface of the epithelial cells lining the airways where they beat continuously to clear mucus and trapped debris and pathogens. While PCD manifests as sinusitis and rhinitis in the upper airways, cilia motility defects lead to a more severe condition in the lower airways, characterised by respiratory mucus entrapment and chronic bacterial infections leading to bronchitis and pneumonia. This results in breathing difficulties and progression to scarred, enlarged airways (bronchiectasis) and increasing deterioration of lung function (Lucas et al., 2014). There is currently no cure for PCD, just symptomatic treatment.

Motile cilia have an internal scaffold structure called the axoneme which is formed of nine microtubule doublets surrounding (in most motile cilia) a central pair of microtubules, (the "9+2" array) (Satir and Christensen, 2007). Cilia contain hundreds of proteins including dynein motor proteins that drive ciliary motility through ATP hydrolysis, by sliding along the outer microtubules (Brokaw and Kamiya, 1987, Burgess et al., 2003). Outer dynein arms regulate ciliary beat frequency, while inner dynein arms and nexin-dynein regulatory complexes link adjacent microtubules, regulating the axonemal waveform and beating pattern (Awata et al., 2015, Heuser et al., 2009). Radial spokes protrude from the peripheral microtubules towards the central pair forming a radial scaffold that also helps mediate ciliary motility through mechanochemical transduction (Zhu et al., 2017). Variants in more than 50 different genes so far are associated with PCD, affecting many structural elements of the axoneme (Legendre et al., 2021) with variants in the outer dynein arm (ODA) heavy chain gene, *DNAH5*, responsible for at least a third of North European PCD cases (Fassad et al., 2020, Hornef et al., 2006).

Research into therapies for PCD is hampered by the lack of robust models that recapitulate the disease phenotype. In vivo, PCD knockout mouse models with Dnah5 variants usually die in utero or postnatally due to situs inversus-related cardiac conditions, or hydrocephalus. Furthermore, these models fail to replicate respiratory phenotypes, such as bronchiectasis (Ibanez-Tallon et al., 2002, Ostrowski et al., 2010, Yin et al., 2019, Lee and Ostrowski, 2021). A mouse model of PCD associated with variants in another outer dynein arm heavy chain, *Dnah11*, was reported to display immotile tracheal cilia with normal ultrastructure and reduced sperm motility, accompanied by gross rhinitis, sinusitis, and otitis media, (Lucas et al., 2012), although no lower airway disease was reported and there are few subsequent reports using this model. A conditional transgenic model of PCD was generated in 6-11-week-old mice in which administration of tamoxifen, induced Cre recombinase expression, excising the axonemal gene *Dnaic1*. This approach avoided the development of hydrocephalus or cardiac conditions and led to symptoms of mucociliary defects in the lung, however, due to the slow turnover of ciliated cells in the airway, mice took up to 6 months to develop PCD symptoms, which included chronic rhinosinusitis (Ostrowski et al., 2010). Other murine models of PCD in which Rsph1 is deleted develop respiratory symptoms characteristic of PCD, but milder than in other PCD mice and with less severe hydrocephalus, although less than one third of mice survive to adulthood (Yin et al., 2019). A recent mouse model study investigated effects of different variants in *Dnaaf5* in a wide range of tissues, reporting occurrence of differential phenotypes in different tissues, with no lung disorder presented in the lower airway unlike the phenotype observed in PCD patients (Horani and Ferkol, 2018).

Patient derived cultures of human basal epithelial cells at an air liquid interface (ALI) display differentiation and ciliogenesis, producing a pseudostratified epithelium that closely mimics the *in vivo* epithelium and thus provide a robust, versatile model for studying PCD biology and potential therapies (Hirst et al., 2010). However, a significant drawback in the use of this model, is that the expansion of primary basal cell cultures is limited to 2-3 passages due to senescence, limiting their long-term use and requiring multiple acquisition of fresh donor samples (Lechner et al., 1982). We have previously shown that transduction of basal epithelial cells with *BMI1*, a polycomb ring finger protein, delays the onset of senescence for at least 20

passages while basal cells retain their capability to differentiate (Munye et al., 2017). *BMI1*-transduced basal cells from the bronchial epithelium of cystic fibrosis donors (CFBE) displayed characteristic ion transport and fluid homeostasis defects in ALI culture and were used to assess physiological correction with an epithelial sodium channel (ENaC)-targeted siRNA-therapy (Tagalakis et al., 2018).

Here, we report the development and characterisation of human PCD cell models, generated by *BMI1* transduction of bronchial and nasal primary basal epithelial cells from PCD donors biallelic for *DNAH5* variants. *BMI1*-transduced basal cells from both healthy controls and *DNAH5* variant patients were expanded in culture at least up to eighteen passages while retaining their ability to differentiate into a pseudostratified, ciliated epithelium with dysmotile cilia that lacked DNAH5 and other outer dynein arm proteins, thus recapitulating key features of PCD. In contrast, *BMI1* transduced basal cells from the bronchial epithelium of healthy individuals displayed abundant ciliation with normal ciliary motility. In characterising these PCD models, the ciliary localisation of axonemal proteins, including DNAH5, DNAI1, RSPH1, CCDC39 and CCDC40, was evaluated, as well as their ultrastructure by transmission electron microscopy. In addition, preliminary studies were performed into the expression and activity of ENaC and CFTR in *BMI1*-transduced PCD cells, ion transport channels that regulate homeostasis in the periciliary liquid layer and play an important role in mucociliary clearance.

RESULTS

Expansion and differentiation of BMI1-transduced PCD basal cells

Nasal and bronchial brushing samples were obtained from PCD donors both biallelic for *DNAH5* variants (Table 1), then primary basal cells derived from patient donor 1 (DNAH5-1-*BMI1*) were cultured in 12-well plates with growth media for basal cell expansion. Cells reached 90% confluency in 7 days and displayed characteristic cobblestone epithelium (**Fig. 1A**). Cells were then transferred to larger wells in 6-well plates at passage 1 (p1) and, 24 hrs post-seeding, were transduced with a lentiviral vector encoding *BMI1*, at multiplicities of infection (MOI) of 1, 4 and 16. Cells were maintained in the wells for the next 7 days then transferred to T75 flasks (p2) and

further expanded in growth media until 90% confluent. BMI1 transduced basal cells at all MOIs displayed characteristic basal epithelial cell morphology like their nontransduced primary cell counterparts, as captured at p2 for donor 1 in (Fig. 1B). Cells obtained from nasal brushing of PCD donor 2 (DNAH5-2) displayed similar behaviour and appearance compared to cells derived from the bronchial region, DNAH5-1 (not shown). The cells transduced at MOI 16 were selected for subsequent experiments based on growth rate studies conducted in NHBE-BMI-1 cells, since this MOI16 showed a constant growth rate for at least 85 days, while non-transduced primary cells grew at a slower rate which declined from day 10 (Fig. S1). Immunofluorescent staining was then performed to assess the expression of airway basal epithelial cell markers, p63, a transcription factor required for epithelial progenitor cell renewal (Melino et al., 2015), and cytokeratin-5 (CK5), a filament protein characteristic of progenitor cells (Voynow et al., 2005). These markers were detected in both NHBE and DNAH5-1 basal cells prior to differentiation in ALI culture (Fig. 1C, D). Positive staining for p63 and CK5, which are both characteristic of progenitor cells, suggests that BMI1-transduced cells retain their pluripotency.

Characterisation of ALI cultures of *BMI1*-transduced PCD airway epithelial cells

ALI cultures were established from *BMI1*-transduced DNAH5-2 and NHBE basal cells, both at p12, and assessed for their epithelial phenotype. Both NHBE cells and DNAH5-2 cells displayed an intact epithelial sheet on transwell membranes at day 35 post air-lift in ALI culture, therefore subsequent experiments were performed at this time point (Fig. 2A) although the epithelium maintained its differentiated appearance for at least 60 days of ALI culture (Fig. 2B). Transepithelial resistance (TEER) values were similar for both DNAH5-2 and NHBE ALI cultures, indicating the development of a functional epithelial barrier (Fig. 2C).

ALI culture imaging and analysis for ciliary beat frequency by high-velocity video microscopy

Cilia on *BMI1*- transduced NHBE cells displayed a ciliary beat frequency (CBF) of approximately 15 Hz at day 35 and day 60 of ALI culture, which is in the normal range (Smith et al., 2012), and a normal ciliary beat pattern (Fig. 2D, supplementary videos 1-4). The cilia in *BMI1*-transduced DNAH5-2 cells, however,

were mostly static, consistent with the phenotype resulting from the lack of outer dynein arms (Fig. 2D, supplementary videos 5-8).

Expression of *DNAH5* was determined by qRT-PCR analysis of total cell mRNA from ALI cultures at 7 day intervals up to day 21 and at day 49. *DNAH5* expression in ALI cultures of both DNAH5-2 and NHBE cells increased from day 7 of ALI until day 49 for both cell lines, with no significant difference in the increase between them (**Fig. 2E**). Thus, *BMI1* transduction had no impact on the pattern of increasing *DNAH5* expression and associated ciliogenesis (Loges et al., 2018).

Characterisation of ciliary proteins in PCD airway epithelial cells

We next analysed the ALI cultures of *BMI1*-transduced PCD cells by immunofluorescent staining for evidence of differentiation by ciliation and mucus production. Immunofluorescent images of ALI cultures of both NHBE and DNAH5-2 cells at day 30 acquired by confocal microscopy, displayed densely ciliated cultures detected by staining for acetylated α tubulin (green), as well as mucus production by secretory cells, detected by staining for the mucin, MUC5B (red) (**Fig. 3A, B**). Immunofluorescent staining was then performed to assess the ciliary localisation of DNAH5 and other proteins involved in cilia structure and motility. DNAH5 (red) was detected in the motile cilia of NHBE cells (**Fig. 4A**) but, consistent with their genotype, was absent from the cilia of both DNAH5-2 and DNAH5-1 cells (**Fig. 4B, Fig. S2**), suggesting impaired ciliary trafficking of the mutant protein.

Immunofluorescent analysis of another outer dynein arm protein, DNAI1, revealed its co-localisation with DNAH5 along the length of the cilia in NHBE cells, and, as expected, its absence from cilia of DNAH5-2 and DNAH5-1 cells since the entire ODA is missing (**Fig. 4C, D, Fig. S3**) (Loges et al., 2018).

Other cilia structural proteins, including the radial spoke protein RSPH1 (**Fig. 5A, B, Fig. S4**) and molecular ruler proteins CCDC39 and CCDC40, were all detected to be localised in both *BMI1*-transduced NHBE and DNAH5-2, DNAH5-1 cilia, indicating they are unaffected by the loss of DNAH5 (**Fig. 6, Fig. S5 & S6**), as expected for non-ODA structural proteins. The loss of ciliary ODAs in ALI cultures of both DNAH5-1 and DNAH5-2 cells was confirmed by TEM analysis of primary cell ALI cultures

before *BMI1* transduction (Fig. 7A, B) as well as in DNAH5-2 cells post *BMI1* transduction, while ODA structures were normal in NHBE cells (Fig. 7C, D).

Comparison of BMI1 Transduced PCD cell characteristics to primary PCD cells

To investigate whether *BMI1* transduced PCD airway epithelial cells retain their phenotype, capacity of growth and differentiation potential over long term, we generated ALI cultures from *BMI1*-transduced basal cells at later passages (p1,15 and p.1,19) and compared them against their primary cell counterparts. ALI cultures established from both p.1,15 and p.1,19 of *BMI-1* transduced DNAH5-1 cells formed intact epithelial sheets on transwells, retaining their epithelial cell morphology similar to that of primary DNAH5-1 cells of p.3 (Fig. S7A). TEER values of p.19 DNAH5-1 *BMI1* cells were slightly higher than the non-transduced cells (Fig. S7B) indicating they retained the ability to form an intact epithelial barrier, despite their high passage number, while ciliary beat frequencies for both were static, retaining their PCD phenotype (Fig. S7C).

TEM analysis of p.1,19 DNAH5-1 *BMI1* cells grown in ALI cultures revealed cilia structures similar to their non transduced primary cell cilia, with missing outer dynein arms (Fig. S7D). In order to assess their proliferation potential over time, *BMI1* transduced DNAH5 cells from different passage numbers, p.1,8 and p.1,12 were maintained in cell culture to 60 days and growth curves plotted. Both p.1,8 and p.1,12 DNAH5 *BMI1* cells displayed similar growth rates, whilst their primary cell counterparts displayed growth arrest after 3 passages (Fig. S7E). These results indicate that *BMI1* transduced PCD cells can retain their proliferation potential long term, retaining similar growth kinetics at later passages. Confocal analysis of DNAH5-1 *BMI-1* transduced late passage cells (p.1,19) cultured in ALI along with the non-transduced primary DNAH5-1 cells to assess differentiation potential showed that the *BMI1* transduced cells of passage 19 were capable of differentiation as non-transduced cells, both displaying less secretory cells with similar level of MUC5AC measured across 6 random fields imaged, with slightly higher percentage of ciliated fields measured in primary DNAH5-1 cultures (Fig. S8).

ENaC and CFTR expression and ion transport activity in PCD cells

The epithelial sodium channel, ENaC, and the anion channel, CFTR, play important roles in regulating not just ion flow but also fluid flow across the epithelium impacting on mucociliary clearance through their effects on depth of the airway surface liquid (ASL), comprising the mucus and periciliary liquid layers (PCL), and the viscosity of the mucus. Therefore, it was important to confirm these ion channels are expressed in BMI1-transduced DNAH5 cells. Ion channel activities were measured as short circuit currents (I_{sc}) of ENaC and CFTR in DNAH5 mutant airway epithelial cells and were compared to BMI1-transduced NHBE and cystic fibrosis cells (CFBE). Spontaneous (basal current) short -circuit current (I_{sc}) was first measured, which revealed differences in net ion transport between the bronchial PCD cells (DNAH5-1) and NHBE cells (Fig. 8A). The change in I_{sc} after application of amiloride to inhibit ENaC (Δ amiloride) was lower in DNAH5-1 cells than in NHBE cells or CFBE cells, indicating less ENaC channel activity in the bronchial PCD cells (Fig. 8A), although Western blot analysis suggested that the major ENaC subunit, α ENaC at least was expressed, at slightly higher levels relative to NHBE cells (Fig. S9). Amiloride induced a greater short circuit current inhibition in CFBE cells than NHBE cells, indicating higher ENaC activity, characteristic of a CF epithelium (Fig. 8A) (Moore and Tarran, 2018). Thus, this data indicates that ENaC channel activity is lower in the ALI cultures of PCD bronchial epithelial cells. Immunofluorescent staining of NHBE and PCD bronchial airway epithelial cells showed that αENaC was distributed in the membrane along the length of the ciliary axonemes in both cell types in similar amounts (Fig. 8B,C), consistent with the Western blot analysis (Fig. S9). Despite the similar ciliary levels of αENaC observed in NHBE and DNAH5-1 cells, total αENaC protein levels by Western blot analysis were higher in both PCD cell lines (DNAH5-1 & DNAH5-2) compared to NHBE cells and CFBE cells, with the latter exhibiting even lower levels of total αENaC protein than NHBEs despite their higher ENaC ion channel activity. Thus, the differences in ENaC activity observed in Ussing chamber analysis of ALI cultures are probably a consequence of regulatory control of ENaC rather than abundance of the protein or distribution of the channel. ENaC is subjected to a complex array of post-translational regulatory processes, including protease activation and CFTR inhibition which has been studied in relation to CF

(Mall, 2020, Matalon et al., 2015), but there is little known of ENaC regulation in relation to ciliary motility in PCD (Wu et al., 2018).

ALI cultures of PCD bronchial epithelial cells displayed greater ΔI_{sc} in response to IBMX/forskolin treatment than in NHBE cells, indicating greater activation of CFTR, while the ΔI_{sc} in response to the CFTR specific inhibitor, CFTR_{inh}-172, was also greater in PCD bronchial epithelium (DNAH5-1) than NHBE epithelium (Fig. 8A). epithelium, as expected, yielded little response to activation with IBMX/forskolin or inhibition with CFTR_{inh}-172, consistent with the absence of CFTR. In addition to higher CFTR ion channel activity in bronchial PCD cells, both PCD cell types in ALI cultures displayed higher levels of CFTR protein than NHBE cells, with both mature (band C) and immature forms (band B) of CFTR present, suggesting the presence of functional CFTR protein (Fig. S9). Analysis of more donor samples is required to explore whether the increased activity and abundance of CFTR in PCD epithelium is a disease specific phenotype. Finally, the inhibitory ΔI_{sc} in response to ouabain was greater in DNAH5-1 cells than in NHBE or CFBE cells. As ouabain inhibits all ion transport processes in airway cells, these data indicate that ion transport activities other than those associated with ENaC and CFTR may be upregulated in PCD cells.

Further studies will be required with cells from a wider range of PCD donors but the striking differences in ENaC and CFTR activity and protein levels of the *BMI1*-transduced bronchial PCD cells used in this study raises questions of whether this may be linked to impaired ciliary function. ENaC and CFTR play central roles in airway surface liquid homeostasis and so we hypothesise that increased CFTR and reduced ENaC activity may enhance hydration of the lung epithelium, compensating partially for the loss of mucociliary clearance in PCD cells. Further studies will be required to explore this hypothesis, but the *BMI1*-transduced basal PCD cells provide a consistent reliable resource for mechanistic studies without having to resample the same donor.

DISCUSSION

Cell culture models that mimic the phenotype of the PCD airway epithelium are useful for studying airway disease mechanisms, to discover new genetic components involved in the disease, and for developing new therapies. There is a shortage of convenient models of PCD that display phenotypes specific to the underlying genetic variants and so we have developed and analysed cell models from two PCD donors with variants in the gene encoding DNAH5, a critical protein in the outer dynein arm which we propose could be useful for research into PCD. Absence of DNAH5 in PCD patients leads to loss of the outer dynein arms (ODA) and ciliary dysmotility.

Basal epithelial cells, obtained from biopsies or airway brushings, are progenitors of the differentiated airway epithelia and can be differentiated in ALI cultures to mimic the human airway in vitro. However, primary basal cells are capable of expansion for only 2-3 passages before losing their differentiation capacity, and so different approaches to enable expansion of these cells, while retaining their differentiation capacity, have been explored. Maintaining basal cells in co-culture with irradiated mouse feeder fibroblast cells with Rho associated protein kinase (ROCK) inhibitor in the medium, results in a high yield of cells in successive passages that differentiate on air-lift in ALI cultures (Butler et al., 2016). However, reports suggest this approach maintains differentiation efficiency only up to 11 passages while cells also display changes in morphology (Reynolds et al., 2016, Suprynowicz et al., 2012). Moreover, the co-culture system is labour-intensive and time consuming and may cause concerns over xenogenicity for downstream studies (Llames et al., 2015). Airway epithelial cells, including those from PCD donors, have been generated from induced pluripotential stem cells (iPSCs) but the process is prolonged, taking several weeks, and laborious (Hawkins et al., 2021). Human bronchial epithelial cells immortalised by simian virus 40 (SV40) large T antigen transformation such as the well-known 16HBE14o- cell line, can form stratified epithelia and tight junctions and are useful for ion transport studies, but fail to produce mucus or cilia (Gruenert et al., 1988), limiting their utility for studies of PCD. Bronchial epithelial cells immortalised with HPVE6/E7 in conjunction with human telomerase reverse transcriptase (hTERT) have karyotypic abnormalities as progressively lose cilia with increasing passage number (Zabner et al., 2003). To resolve the problem of viral oncogenes, a

significant advance was made by transducing human bronchial epithelial cells with the mouse polycomb ring finger oncogene (*BMI1*) and hTERT, creating cell lines of normal karyotype and no nuclear abnormalities, although differentiation was defective with mostly mucus-producing cells and only few ciliated cells (Fulcher et al., 2009). We have reported previously transduction of human primary bronchial epithelial cells from healthy (Munye et al., 2017) and CF individuals (Tagalakis et al., 2018) with human *BMI1* alone that resolved these problems, establishing cell lines with a normal karyotype, electrophysiological properties, mucociliary functionality and sustained proliferative and differentiation properties for up to 25 passages (18).

In this study, *BMI-1* transduced DNAH5 PCD cell models were established from both bronchoscopy and nasal brushings, demonstrating extended capacity for replication and differentiation. *BMI1*-transduced cells expressed the basal cell markers p63 and CK5 indicating they retained their pluripotency. Upon seeding basal cells on porous inserts with differentiation media at the basal side and air exposure at the apical side, pseudostratified airway epithelia were generated with ciliated and mucusproducing cells, even with repeated passaging of the basal cells. *BMI-1*-transduced PCD basal cells could be expanded for at least 19 passages while retaining their differentiation capacity and could be returned to culture after storage in liquid nitrogen. In this study we have shown that *BMI1* transduction of PCD basal epithelial cells provides a robust, patient-derived cell model for long-term expansion and differentiation in ALI cultures.

The *BMI1*-transduced DNAH5 cells in ALI culture accurately recapitulate the PCD phenotype, with static and dysmotile cilia, while cilia in *BMI1*-transduced NHBE airway cells derived from healthy donors display normal ciliary motility. Immunostaining showed that DNAH5 and its associated intermediate chain partner (DNAI1) were absent from the cilia of DNAH5-defective cells. In contrast, non-ODA proteins such as the nexins, CCDC39 and CCDC40, and the radial spoke protein, RSPH1 were detected in the cilia of these cells (Enuka et al., 2012, Loges et al., 2018, Fliegauf et al., 2005). *DNAH5* mRNA transcripts were present in PCD cells and increased during ciliogenesis in ALI culture, like NHBE cells. The presence of mRNA in differentiating DNAH5-2 cells that contain biallelic nonsense mutations suggests that DNAH5 mRNA was not fully depleted by nonsense-mediated decay

(NMD). Transcripts with premature termination codons (PTC) can be stable to NMD enabling translation of truncated products (Kim et al., 2017). The absence of DNAH5 protein in the cilia despite the presence of *DNAH5* mRNA transcripts in DNAH5-2 cells, suggests the inability of the truncated protein to be trafficked into the cilium as was the case for DNAH5-1 cells that contained one allelic nonsense mutation and one missense mutation (Table1).

ENaC was detected in the membrane of the motile cilia of both DNAH5 cells and NHBE cells, where it is ideally placed to regulate airway surface liquid (ASL) volume, which bathes the cilia (Hanukoglu and Hanukoglu, 2016). Analysis of the electrophysiological properties of the bronchial DNAH5 BMI1 epithelium at day 30 of ALI culture revealed significantly decreased responses to amiloride compared to ALI cultures of NHBE cells and CFBE cells, indicating decreased ENaC activity in the PCD ALI culture. The PCD epithelium from ALI, however, appeared to contain similar amounts of ciliary $\alpha ENaC$ protein to NHBE ALI cultures, suggesting regulatory process may have led to reduced ENaC activity. ENaC is regulated by proteases (Myerburg et al., 2010) but there is growing evidence that ENaC is activated by mechanical forces such as hydrostatic pressure or membrane stretching as well as shear-stress caused by fluid flow in several organs and cell types including oocytes, endothelium and kidney (Shi et al., 2013), and evidence of fluidflow shear stress activation of ENaC in lung cells (Fronius et al., 2010). So the lack of ciliary movement and loss of fluid flow may be playing roles in regulating ENaC in ALI cultures of the PCD-BMI-1 cells. CFTR is also thought to play a role in regulating ENaC activity (Rooj et al., 2021) and, interestingly, in our PCD cells, CFTR activity was elevated in ALI cultures of bronchial PCD line compared to NHBE cells. These studies were performed with only one PCD cell type and so it is not possible to draw firm conclusions on ion transport properties of the PCD phenotype but they do suggest this might be an area that requires further investigation with larger sample numbers (Tosoni et al., 2016).

Loss of ENaC combined with enhanced CFTR activity would be expected to increase ASL volume although a previous study reported that PCD cells have a normal ASL depth (Tarran et al., 2006). However, those experiments focused on measuring the

ability of the PCD cells to restore ASL volume upon addition of PBS and did not examine ENaC activity levels during the process. Interestingly, a clinical trial was performed with the nebulised ENaC inhibitor VX-371/ P-1037 and hypertonic saline, with the aim of clearing mucus obstructions by increasing hydration in the airways (clinicaltrials.gov; identifier NCT02871778). Our studies suggest that, although αENaC protein levels are elevated in PCD; channel activity is not, this might be the result of regulation of ENaC activity which may help to increase airway surface fluid and to enhance mucus clearance, which is impaired in PCD. The *BMI1*-transduced PCD, NHBE and CFBE cells described here will enable further studies of the interrelationship of ion and fluid homeostasis in the airways in relation to ciliary activity.

The *BMI1*-transduced basal cells from PCD donors lacking DNAH5 described here offer a useful resource for the study of PCD biology and are capable of long-term culture and differentiation. Biobanking of PCD cells offers a potentially useful resource for studies into PCD biology and therapies and the *BMI1* transduction process could enhance the utility of stored cells as they reliably recapitulate the disease phenotype *in vitro*. Recent studies have highlighted differential gene expression profiles that were identified in airway cells of PCD donors with DNAH5 variations, which were suggested to potentially provide a compensatory mechanism for loss of DNAH5 function that could be investigated using our model (Koenitzer et al., 2024, Yang et al., 2022). The method is simple, and reproducible in the culture of patient-specific airway basal cells which renders them a suitable system for use in the development of novel therapies ranging from read through drugs to genetic therapies (Paff et al., 2021).

MATERIALS AND METHODS

Subjects

All patient samples were obtained with the individual's consent under local and national ethical approvals (London - Bloomsbury Research Ethics Committee 08/H0713/82, Northwest - Liverpool Central Research Ethics Committee 14/NW/0128). Patient genotypes were confirmed previously with variant

nomenclature according to DNAH5 transcript NM_001369.3. Airway epithelial cells harbouring predicted loss-of-function DNAH5 variants were collected from two PCD donors, one carrying two nonsense variants and the other carrying a frameshift variant and a nonsense variant (Table1). All variant alleles are known to be pathogenic (www.nlm.nih.gov/clinvar). Normal human bronchial epithelial cells (NHBE) were obtained from The Royal Institution for the Advancement of Learning/McGill University, Montreal, Canada at passage no 1. CFBE cells, homozygous for the common Δ F508 variant were obtained from Epithelix (Geneva, Switzerland).

BMI1 transduction of primary airway epithelial cells

Primary basal cells from bronchial or nasal brushings of the two PCD DNAH5 patients were expanded on 12-well plates in PneumaCult-ExTM growth medium (StemCell Technologies, Cambridge, UK). Cells were harvested and seeded at 1 x 10⁵ cells/well in 6-well plates in PneumaCult-ExTM growth medium (StemCell Technologies, Cambridge, UK). The next day, cells were transduced using LV-BMI PURO virus (Munye et al., 2017) in Opti-MEM (Thermo Fisher Scientific, UK) at multiplicities of infection (MOI) of 1, 4 and 16. BMI1 plasmid map is shown in Fig. S10. Lentivirus preparation and titration protocol were performed as described previously (Maeshima et al., 2024). PneumaCult-ExTM growth media (StemCell Technologies, UK) was added to the cells the following day then media was changed every two days until the cells reached 90% confluence, typically at day 7. Cells were harvested and transferred into T75 flasks pre-coated with 10% Collagen I (Coll) (PureCol® Bovine Collagen Solution, Type I, Advanced BioMatrix, San Diego, CA, USA) for further expansion in PneumaCult-ExTM growth medium (StemCell Technologies, Cambridge, UK). All tissue culture plasticware was coated with Coll, prior to seeding the cells.

Air Liquid Interphase Cultures (ALI)

1 million cells were plated per 12 mm diameter well on collagen-coated transwell or snapwell inserts (Polyester (PET) Membrane Transwell-Clear Inserts, Corning, Corning Inc. Life Sciences, Flintshire, UK). They were grown up to 5 days in PneumaCult ExTM growth medium on both apical and basal sides (StemCell Technologies, Cambridge, UK). After 5 days the apical media was removed and growth medium was changed to ALI culture medium (PneumaCult ALITM, StemCell Technologies, Cambridge, UK) for differentiation. For this the media was changed every 2 days and cells were analysed after day 30 of differentiation.

Immunofluorescence staining and confocal analysis

Cells on transwell membranes were fixed in 4% paraformaldehyde (PFA) for 10 minutes, washed in phosphate-buffered saline (PBS) (Sigma-Aldrich, Gillingham, UK), permeabilized with Triton-X100 (0.2 %) (Bio-Rad, Hertfordshire, UK) in PBS for 10 minutes, then washed with PBS three times for 5 min per wash. Membranes were blocked with 5% goat serum and 1 mg/mL bovine serum albumin (BSA) in PBS for 30 minutes at room temperature (RT), followed by overnight incubation with primary antibodies at 4°C. Samples were washed three times with BSA (0.1 mg/ml) in PBS for 5 min per wash, followed by incubation with secondary antibodies for one hr at RT. After three more wash steps with BSA (0.1 mg/ml) in PBS, nuclear staining was performed using DAPI Solution, (Thermofisher Scientific, Hemel Hempstead UK). Transwell membranes were cut out of holders using a scalpel and transferred onto slides with the apical surface facing up and mounted using n-Propyl gallate (0.5 % n-Propyl gallate in glycerol, 0.1 M Tris-Cl pH 8.0).

Primary antibodies used were: mouse anti-acetylated α tubulin (TUBAIA ace-40Lys; 66 200-1 Ig; Proteintech, Manchester, UK); rabbit anti-DNAH5, (HPA037470, Lot. B1144222) and rabbit anti-CCDC39 IgG, (HPA 035364, Lot A106506) from Atlas Antibodies, Bromma, Sweden; rabbit anti-CCDC40, (HPA 022974; diluted 1:1000), rabbit anti-RSPH1, (HPA 017382; diluted 1:100), rabbit anti-DNAI1, (HPA 028305; diluted 1:200) and rabbit anti-MUC5B, (HPA008246) from Sigma-Aldrich Gillingham, UK; mouse anti-cytokeratin 5, (anti-CK5), (ab17130) and rabbit anti-p63, (ab53039) from Abcam, Cambridge, UK; and rabbit anti-αENaC (SCNN1A) (PA1-920A; ThermoFisher Scientific, Hemel Hempstead, UK) (all were diluted 1:500 other than as stated). Secondary antibodies were Alexa Fluor 488 F(ab')2 fragment of goat antimouse IgG (H1L) and Alexa Fluor 633 goat anti-rabbit IgG (H1L) (all 1:1000) (both

from Molecular Probes, Life Technologies, Paisley, UK). For primary cell IF data conjugated antibodies were used as anti-acetylated α tubulin (6-11B-1) AF647 conjugated, (sc-23950, Lot.K0724) from Santa Cruz Biotechnology, Dallas, US and mouse anti MUC5AC AF488, Alexa fluor, (NBP2-32732, Lot. D185610) from Biotechne, Minnesota, US. Samples were imaged using a Zeiss LSM710 Confocal microscope (Zeiss, Cambridge, UK) at 63x objective. Samples were imaged using ZEN blue software, with multiple z-sections taken through the thickness of the cell at 500 nm intervals. Maximum projectioµµns of z-stacks were recorded and analysed using Fiji Iµage J software and ciliary ENaC was quantified using Imaris software, detecting each ciliary axoneme in z- stacks and automatically drawing boundaries around the cilia, with a diameter < 0.3 µm set to detect each axonemal microtubule. (Oxford Instruments, Oxford, UK).

qRT-PCR

Total cell RNA was extracted from cell using a RNeasy mini kit (Qiagen, Crawley, UK). Complementary DNA (cDNA) synthesis and quantitative PCR (qPCR) were performed from RNA samples using Sensi Fast SYBR Hi-ROX One step kit (Bioline, London, UK) in a Bio-Rad CFX96 thermal cycler (Bio-Rad, Watford UK). DNAH5 (Hs00292485 m1) and β -actin (Hs01060665-g1) reference gene expression, as quantified by Taqman primers and probes (Applied Biosystems, Warrington, Cheshire, UK). PCR was performed at 45°C for 20 min, 95°C for 2 min followed by 40 cycles at 95 °C for 15 sec and 60 °C for 1 min. Relative gene expression levels were determined using the delta-delta Ct (2 $^{-\Delta\Delta Ct}$) method (Livak and Schmittgen, 2001).

Ciliary Motility Analysis

Ciliary beat frequency (CBF), beat pattern and other morphological features of the cilia were analysed by high-speed video microscopy (HSVM), as described previously (Thomas et al., 2010). Briefly, cells were suspended in HEPES (20 mM) buffered medium 199 containing penicillin (50 μ g/ml), streptomycin (50 μ g/ml) and Fungizone (1 μ g/ml). Strips of ciliated epithelium (37°C) were imaged using a x100

objective and digitally recorded using a high-speed camera. Ciliary activity was recorded at a rate of 500 frames per second (fps) and played back at reduced frame rates for CBP and CBF analysis. CBF was calculated using the following equation [CBF =(500/number of frames for 10 ciliary beats) x 10] and a mean CBF was reported from a minimum of 6 measurements on independent ciliated strips. Cilia movies were taken from 10 strips of ciliated epithelium at 500 frames per second. The normal range of CBF was 10-14Hz while immotile cilia have a CBF of 0 Hz. The ciliary beat pattern was defined as normal, dyskinetic or immotile as viewed from the side profile. Dyskinetic cilia have abnormal beating, such as bending failure or display a twitching motion. The % frequency of dyskinesia was calculated as the number of dyskinetic and immotile cilia per total number of measurements.

Transmission electron microscopy

The ciliated epithelium for TEM was fixed in 3-4% glutaraldehyde and prepared, imaged and analysed in a blinded fashion as described previously (Stannard et al., 2010). The percentage of ultrastructural defects was determined by analysis of cilia in cross section. The number of cross sections analysed (typically 300 cilia) was dictated by the size and secondary damage within the fixed sample. Common defects included missing outer and inner dynein arms alone or together, truncated outer dynein arms and microtubular disarrangement.

Electrophysiology

Cells were grown on Costar Snapwell™ Clear permeable supports (Corning Life Sciences, Flintshire, UK) in ALI culture (PneumaCult ALI™, StemCell Technologies, Cambridge, UK) for 30 days, PCD cell lines from successive passages of p10-p18 were utilised in electrophysiology studies. Cells were rinsed twice with growth media (PneumaCult Ex™, StemCell Technologies, Cambridge, UK) two days prior to analysis. Cells were then mounted in Ussing chambers and 5 mL isotonic physiological salt solution buffer (PSS) was added to either side of the membrane. PSS was composed of NaCl (117nM), NaHCO₃ (25 nM), KCl (4.7 nM), MgSO₄ (1.2 nM), KH₂PO₄ (1.2nM), CaCl₂ (2.5 nM) and D-glucose (11.0 nM), pH7.4. The solution

was maintained at 37°C and continuously bubbled with 21% O_2 +5% CO_2 premixed gas throughout the course of the experiment. The epithelium was clamped at 0 mV and short-circuit current (Isc) was measured. Every 30 s, a 2-mV pulse was applied to enable calculation of transepithelial resistance (TEER) as described (Tagalakis et al., 2018). Spontaneous short circuit current (I_{sc}) was measured before addition of the drugs and after addition of each drug to evaluate drug response by observing change in I_{sc} (ΔI_{sc}). Amiloride,10 μ M, (apical) was used to inhibit ENaC, forskolin, 10 μ M and IBMX 10mM (bilateral) to elevate cAMP and activate CFTR, CFTR_{inh}172, 10 μ M (apical) to inhibit CFTR and ouabain, 1mM (basolateral) to inhibit Na⁺K⁺ATPase (all drugs were obtained from Sigma-Aldrich).

Western Blot

Cells in ALI culture on PET transwell inserts (Corning Life Sciences, Flintshire, UK) were lysed using RIPA buffer with protease inhibitor cocktail (ThermoFisher Scientific, Hemel Hempstead, UK) and incubated on ice for 15 min followed by 15 min centrifugation at 17,000 x g at 4° C. The supernatant was transferred to microfuge tubes (Eppendorf, Stevenage, UK) and protein concentration of the lysate was measured using a bicinchoninic acid (BCA) assay (ThermoFisher Scientific, Hemel Hempstead, UK). Protein samples were mixed with 6x loading buffer supplemented with denaturing reagent, (0.375 M Tris-HCl pH 6.8, 10% (w/v) SDS, 30% (v/v) glycerol, 0.6 M dithiothreitol (DTT), 0.05% (w/v) bromophenol blue) and incubated at 37°C for 30 min prior to loading. 17 µg total protein was loaded into each well of NuPAGE 4-12% Bis-Tris protein gels (ThermoFisher Scientific, Hemel Hempstead, UK). Gel electrophoresis was performed in MOPS buffer for 90 min at 80mA in a XCell SureLockTM Mini-Cell (ThermoFisher Scientific, Hemel Hempstead, UK). Proteins were transferred to polyvinylidene difluoride (PVDF) membrane (Millipore, Watford, UK) in transfer buffer (25mM Tris base, 192mM glycine, 20% (v/v) methanol) using a Bio-Rad Mini trans-Blot tank (Bio-Rad Laboratories, Watford, UK) for 70 min at 140V. The membrane was then blocked with 5% dried milk powder in TBS-T (50mM Tris-base pH 7.5, 150mM NaCl, 0.2% Tween-20) for 1 hr at room temperature. The membrane was incubated with mouse anti-CFTR antibody (AB596, from S. Randell, University of North Carolina, USA) or rabbit anti-αENaC (SCNN1A) (PA1-920A; ThermoFisher Scientific, Hemel Hempstead, UK) both diluted 1/1,000, or

mouse anti-GAPDH (diluted 1/10,000) in 5% dried milk in TBS-T overnight at 4°C followed by three washes with TBS-T 10 min each. The membrane was then incubated with rabbit anti-mouse horseradish peroxidase (HRP)-conjugated secondary antibody (1: 10,000) (Dako, Ely, UK) or goat anti-rabbit HRP-conjugated secondary antibody for 1 hour in blocking buffer followed by three washes in TBS-T, 10 min each. The blot was developed for imaging using high sensitivity ECL solution (Pierce ECL plus, ThermoFisher Scientific, Hemel Hempstead, UK) and imaged using a ChemiDoc™ MP Imaging System (Bio-Rad, Watford, UK).

Acknowledgements

We thank Amelia Shoemark (Imperial College and University of Dundee), Ranjit Rai (Imperial College) and Andrew Rutman (University of Leicester) for TEM analysis. We thank Newlife: The Charity for Disabled Children (Registered Charity Number: 1170125 in England & Wales) and the National Institute for Health Research Biomedical Research Centre at Great Ormond Street Hospital for Children NHS Foundation Trust and University College London, for funding this work.

References

- AWATA, J., SONG, K., LIN, J., KING, S. M., SANDERSON, M. J., NICASTRO, D. & WITMAN, G. B. 2015. DRC3 connects the N-DRC to dynein g to regulate flagellar waveform. *Mol Biol Cell*, 26, 2788-800.
- BROKAW, C. J. & KAMIYA, R. 1987. Bending patterns of Chlamydomonas flagella: IV.

 Mutants with defects in inner and outer dynein arms indicate differences in dynein arm function. *Cell Motil Cytoskeleton*, 8, 68-75.
- BURGESS, S. A., WALKER, M. L., SAKAKIBARA, H., KNIGHT, P. J. & OIWA, K. 2003. Dynein structure and power stroke. *Nature*, 421, 715-8.
- BUTLER, C. R., HYNDS, R. E., GOWERS, K. H., LEE DDO, H., BROWN, J. M., CROWLEY, C.,

 TEIXEIRA, V. H., SMITH, C. M., URBANI, L., HAMILTON, N. J., THAKRAR, R. M., BOOTH,

 H. L., BIRCHALL, M. A., DE COPPI, P., GIANGRECO, A., O'CALLAGHAN, C. & JANES, S.

 M. 2016. Rapid Expansion of Human Epithelial Stem Cells Suitable for Airway Tissue

 Engineering. *Am J Respir Crit Care Med*, 194, 156-68.

- ENUKA, Y., HANUKOGLU, I., EDELHEIT, O., VAKNINE, H. & HANUKOGLU, A. 2012. Epithelial sodium channels (ENaC) are uniformly distributed on motile cilia in the oviduct and the respiratory airways. *Histochem Cell Biol*, 137, 339-53.
- FASSAD, M. R., PATEL, M. P., SHOEMARK, A., CULLUP, T., HAYWARD, J., DIXON, M., ROGERS, A. V., OLLOSSON, S., JACKSON, C., GOGGIN, P., HIRST, R. A., RUTMAN, A., THOMPSON, J., JENKINS, L., AURORA, P., MOYA, E., CHETCUTI, P., O'CALLAGHAN, C., MORRIS-ROSENDAHL, D. J., WATSON, C. M., WILSON, R., CARR, S., WALKER, W., PITNO, A., LOPES, S., MORSY, H., SHOMAN, W., PEREIRA, L., CONSTANT, C., LOEBINGER, M. R., CHUNG, E. M. K., KENIA, P., RUMMAN, N., FASSEEH, N., LUCAS, J. S., HOGG, C. & MITCHISON, H. M. 2020. Clinical utility of NGS diagnosis and disease stratification in a multiethnic primary ciliary dyskinesia cohort. *J Med Genet*, 57, 322-330.
- FLIEGAUF, M., OLBRICH, H., HORVATH, J., WILDHABER, J. H., ZARIWALA, M. A., KENNEDY, M., KNOWLES, M. R. & OMRAN, H. 2005. Mislocalization of DNAH5 and DNAH9 in respiratory cells from patients with primary ciliary dyskinesia. *Am J Respir Crit Care Med*, 171, 1343-9.
- FRONIUS, M., BOGDAN, R., ALTHAUS, M., MORTY, R. E. & CLAUSS, W. G. 2010. Epithelial Na+channels derived from human lung are activated by shear force. *Respir Physiol Neurobiol*, 170, 113-9.
- FULCHER, M. L., GABRIEL, S. E., OLSEN, J. C., TATREAU, J. R., GENTZSCH, M., LIVANOS, E., SAAVEDRA, M. T., SALMON, P. & RANDELL, S. H. 2009. Novel human bronchial epithelial cell lines for cystic fibrosis research. *Am J Physiol Lung Cell Mol Physiol*, 296, L82-91.
- GRUENERT, D. C., BASBAUM, C. B., WELSH, M. J., LI, M., FINKBEINER, W. E. & NADEL, J. A. 1988. Characterization of human tracheal epithelial cells transformed by an origin-defective simian virus 40. *Proc Natl Acad Sci U S A,* 85, 5951-5.
- HANUKOGLU, I. & HANUKOGLU, A. 2016. Epithelial sodium channel (ENaC) family:

 Phylogeny, structure-function, tissue distribution, and associated inherited diseases. *Gene*, 579, 95-132.
- HAWKINS, F. J., SUZUKI, S., BEERMANN, M. L., BARILLA, C., WANG, R., VILLACORTA-MARTIN, C., BERICAL, A., JEAN, J. C., LE SUER, J., MATTE, T., SIMONE-ROACH, C., TANG, Y., SCHLAEGER, T. M., CRANE, A. M., MATTHIAS, N., HUANG, S. X. L., RANDELL, S. H.,

- WU, J., SPENCE, J. R., CARRARO, G., STRIPP, B. R., RAB, A., SORSHER, E. J., HORANI, A., BRODY, S. L., DAVIS, B. R. & KOTTON, D. N. 2021. Derivation of Airway Basal Stem Cells from Human Pluripotent Stem Cells. *Cell Stem Cell*, 28, 79-95 e8.
- HEUSER, T., RAYTCHEV, M., KRELL, J., PORTER, M. E. & NICASTRO, D. 2009. The dynein regulatory complex is the nexin link and a major regulatory node in cilia and flagella. *J Cell Biol*, 187, 921-33.
- HIRST, R. A., RUTMAN, A., WILLIAMS, G. & O'CALLAGHAN, C. 2010. Ciliated air-liquid cultures as an aid to diagnostic testing of primary ciliary dyskinesia. *Chest*, 138, 1441-7.
- HORANI, A. & FERKOL, T. W. 2018. Advances in the Genetics of Primary Ciliary Dyskinesia: Clinical Implications. *Chest*, 154, 645-652.
- HORNEF, N., OLBRICH, H., HORVATH, J., ZARIWALA, M. A., FLIEGAUF, M., LOGES, N. T., WILDHABER, J., NOONE, P. G., KENNEDY, M., ANTONARAKIS, S. E., BLOUIN, J. L., BARTOLONI, L., NUSSLEIN, T., AHRENS, P., GRIESE, M., KUHL, H., SUDBRAK, R., KNOWLES, M. R., REINHARDT, R. & OMRAN, H. 2006. DNAH5 mutations are a common cause of primary ciliary dyskinesia with outer dynein arm defects. *Am J Respir Crit Care Med*, 174, 120-6.
- IBANEZ-TALLON, I., GOROKHOVA, S. & HEINTZ, N. 2002. Loss of function of axonemal dynein Mdnah5 causes primary ciliary dyskinesia and hydrocephalus. *Hum Mol Genet,* 11, 715-21.
- KIM, W. K., YUN, S., KWON, Y., YOU, K. T., SHIN, N., KIM, J. & KIM, H. 2017. mRNAs containing NMD-competent premature termination codons are stabilized and translated under UPF1 depletion. *Sci Rep*, 7, 15833.
- KOENITZER, J. R., GUPTA, D. K., TWAN, W. K., XU, H., HADAS, N., HAWKINS, F. J.,

 BEERMANN, M. L., PENNY, G. M., WAMSLEY, N. T., BERICAL, A., MAJOR, M. B.,

 DUTCHER, S. K., BRODY, S. L. & HORANI, A. 2024. Transcriptional analysis of primary

 ciliary dyskinesia airway cells reveals a dedicated cilia glutathione pathway. *JCI Insight*, 9.
- LECHNER, J. F., HAUGEN, A., MCCLENDON, I. A. & PETTIS, E. W. 1982. Clonal growth of normal adult human bronchial epithelial cells in a serum-free medium. *In Vitro*, 18, 633-42.

- LEE, L. & OSTROWSKI, L. E. 2021. Motile cilia genetics and cell biology: big results from little mice. *Cell Mol Life Sci*, 78, 769-797.
- LEGENDRE, M., ZARAGOSI, L. E. & MITCHISON, H. M. 2021. Motile cilia and airway disease. Semin Cell Dev Biol, 110, 19-33.
- LIVAK, K. J. & SCHMITTGEN, T. D. 2001. Analysis of relative gene expression data using real-time quantitative PCR and the 2(-Delta Delta C(T)) Method. *Methods*, 25, 402-8.
- LLAMES, S., GARCIA-PEREZ, E., MEANA, A., LARCHER, F. & DEL RIO, M. 2015. Feeder Layer Cell Actions and Applications. *Tissue Eng Part B Rev*, 21, 345-53.
- LOGES, N. T., ANTONY, D., MAVER, A., DEARDORFF, M. A., GULEC, E. Y., GEZDIRICI, A., NOTHE-MENCHEN, T., HOBEN, I. M., JELTEN, L., FRANK, D., WERNER, C., TEBBE, J., WU, K., GOLDMUNTZ, E., CUTURILO, G., KROCK, B., RITTER, A., HJEIJ, R., BAKEY, Z., PENNEKAMP, P., DWORNICZAK, B., BRUNNER, H., PETERLIN, B., TANIDIR, C., OLBRICH, H., OMRAN, H. & SCHMIDTS, M. 2018. Recessive DNAH9 Loss-of-Function Mutations Cause Laterality Defects and Subtle Respiratory Ciliary-Beating Defects. *Am J Hum Genet*, 103, 995-1008.
- LUCAS, J. S., ADAM, E. C., GOGGIN, P. M., JACKSON, C. L., POWLES-GLOVER, N., PATEL, S. H., HUMPHREYS, J., FRAY, M. D., FALCONNET, E., BLOUIN, J. L., CHEESEMAN, M. T., BARTOLONI, L., NORRIS, D. P. & LACKIE, P. M. 2012. Static respiratory cilia associated with mutations in Dnahc11/DNAH11: a mouse model of PCD. *Hum Mutat*, 33, 495-503.
- LUCAS, J. S., BURGESS, A., MITCHISON, H. M., MOYA, E., WILLIAMSON, M., HOGG, C. & NATIONAL PCD SERVICE, U. K. 2014. Diagnosis and management of primary ciliary dyskinesia. *Arch Dis Child*, 99, 850-6.
- MAESHIMA, R., JACOBS, A. I., DALBAY, M. T. & HART, S. L. 2024. BMI1 Transduction of Human Airway Epithelial Cells for Expansion of Proliferation and Differentiation. *Methods Mol Biol,* 2725, 225-237.
- MALL, M. A. 2020. ENaC inhibition in cystic fibrosis: potential role in the new era of CFTR modulator therapies. *Eur Respir J*, 56.
- MATALON, S., BARTOSZEWSKI, R. & COLLAWN, J. F. 2015. Role of epithelial sodium channels in the regulation of lung fluid homeostasis. *Am J Physiol Lung Cell Mol Physiol*, 309, L1229-38.

- MELINO, G., MEMMI, E. M., PELICCI, P. G. & BERNASSOLA, F. 2015. Maintaining epithelial stemness with p63. *Sci Signal*, 8, re9.
- MOORE, P. J. & TARRAN, R. 2018. The epithelial sodium channel (ENaC) as a therapeutic target for cystic fibrosis lung disease. *Expert Opin Ther Targets*, 22, 687-701.
- MUNYE, M. M., SHOEMARK, A., HIRST, R. A., DELHOVE, J. M., SHARP, T. V., MCKAY, T. R., O'CALLAGHAN, C., BAINES, D. L., HOWE, S. J. & HART, S. L. 2017. BMI-1 extends proliferative potential of human bronchial epithelial cells while retaining their mucociliary differentiation capacity. *Am J Physiol Lung Cell Mol Physiol*, 312, L258-L267.
- MYERBURG, M. M., HARVEY, P. R., HEIDRICH, E. M., PILEWSKI, J. M. & BUTTERWORTH, M. B. 2010. Acute regulation of the epithelial sodium channel in airway epithelia by proteases and trafficking. *Am J Respir Cell Mol Biol*, 43, 712-9.
- OSTROWSKI, L. E., YIN, W., ROGERS, T. D., BUSALACCHI, K. B., CHUA, M., O'NEAL, W. K. & GRUBB, B. R. 2010. Conditional deletion of dnaic1 in a murine model of primary ciliary dyskinesia causes chronic rhinosinusitis. *Am J Respir Cell Mol Biol*, 43, 55-63.
- PAFF, T., OMRAN, H., NIELSEN, K. G. & HAARMAN, E. G. 2021. Current and Future Treatments in Primary Ciliary Dyskinesia. *Int J Mol Sci*, 22.
- REYNOLDS, S. D., RIOS, C., WESOLOWSKA-ANDERSEN, A., ZHUANG, Y., PINTER, M., HAPPOLDT, C., HILL, C. L., LALLIER, S. W., COSGROVE, G. P., SOLOMON, G. M., NICHOLS, D. P. & SEIBOLD, M. A. 2016. Airway Progenitor Clone Formation Is Enhanced by Y-27632-Dependent Changes in the Transcriptome. *Am J Respir Cell Mol Biol*, 55, 323-36.
- ROOJ, A. K., CORMET-BOYAKA, E., CLARK, E. B., QADRI, Y. J., LEE, W., BODDU, R., AGARWAL, A., TAMBI, R., UDDIN, M., PARPURA, V., SORSCHER, E. J., FULLER, C. M. & BERDIEV, B. K. 2021. Association of cystic fibrosis transmembrane conductance regulator with epithelial sodium channel subunits carrying Liddle's syndrome mutations. *Am J Physiol Lung Cell Mol Physiol*, 321, L308-L320.
- SATIR, P. & CHRISTENSEN, S. T. 2007. Overview of structure and function of mammalian cilia. *Annu Rev Physiol*, 69, 377-400.
- SHI, S., CARATTINO, M. D., HUGHEY, R. P. & KLEYMAN, T. R. 2013. ENaC regulation by proteases and shear stress. *Curr Mol Pharmacol*, 6, 28-34.

- SMITH, C. M., DJAKOW, J., FREE, R. C., DJAKOW, P., LONNEN, R., WILLIAMS, G., POHUNEK, P., HIRST, R. A., EASTON, A. J., ANDREW, P. W. & O'CALLAGHAN, C. 2012. ciliaFA: a research tool for automated, high-throughput measurement of ciliary beat frequency using freely available software. *Cilia*, 1, 14.
- STANNARD, W. A., CHILVERS, M. A., RUTMAN, A. R., WILLIAMS, C. D. & O'CALLAGHAN, C. 2010. Diagnostic testing of patients suspected of primary ciliary dyskinesia. *Am J Respir Crit Care Med*, 181, 307-14.
- SUPRYNOWICZ, F. A., UPADHYAY, G., KRAWCZYK, E., KRAMER, S. C., HEBERT, J. D., LIU, X., YUAN, H., CHELUVARAJU, C., CLAPP, P. W., BOUCHER, R. C., JR., KAMONJOH, C. M., RANDELL, S. H. & SCHLEGEL, R. 2012. Conditionally reprogrammed cells represent a stem-like state of adult epithelial cells. *Proc Natl Acad Sci U S A*, 109, 20035-40.
- TAGALAKIS, A. D., MUNYE, M. M., IVANOVA, R., CHEN, H., SMITH, C. M., ALDOSSARY, A. M., ROSA, L. Z., MOULDING, D., BARNES, J. L., KAFETZIS, K. N., JONES, S. A., BAINES, D. L., MOSS, G. W. J., O'CALLAGHAN, C., MCANULTY, R. J. & HART, S. L. 2018. Effective silencing of ENaC by siRNA delivered with epithelial-targeted nanocomplexes in human cystic fibrosis cells and in mouse lung. *Thorax*, 73, 847-856.
- TARRAN, R., TROUT, L., DONALDSON, S. H. & BOUCHER, R. C. 2006. Soluble mediators, not cilia, determine airway surface liquid volume in normal and cystic fibrosis superficial airway epithelia. *J Gen Physiol*, 127, 591-604.
- THOMAS, B., RUTMAN, A., HIRST, R. A., HALDAR, P., WARDLAW, A. J., BANKART, J., BRIGHTLING, C. E. & O'CALLAGHAN, C. 2010. Ciliary dysfunction and ultrastructural abnormalities are features of severe asthma. *J Allergy Clin Immunol*, 126, 722-729 e2.
- TOSONI, K., CASSIDY, D., KERR, B., LAND, S. C. & MEHTA, A. 2016. Using Drugs to Probe the Variability of Trans-Epithelial Airway Resistance. *PLoS One,* 11, e0149550.
- VOYNOW, J. A., FISCHER, B. M., ROBERTS, B. C. & PROIA, A. D. 2005. Basal-like cells constitute the proliferating cell population in cystic fibrosis airways. *Am J Respir Crit Care Med*, 172, 1013-8.
- WU, D., BOUCHER, R. C., BUTTON, B., ELSTON, T. & LIN, C. L. 2018. An integrated mathematical epithelial cell model for airway surface liquid regulation by mechanical forces. *J Theor Biol*, 438, 34-45.

- YANG, W., CHEN, L., GUO, J., SHI, F., YANG, Q., XIE, L., LU, D., LI, Y., LUO, J., WANG, L., QIU, L., CHEN, T., LI, Y., ZHANG, R., CHEN, L., XU, W. & LIU, H. 2022. Multiomics Analysis of a DNAH5-Mutated PCD Organoid Model Revealed the Key Role of the TGF-beta/BMP and Notch Pathways in Epithelial Differentiation and the Immune Response in DNAH5-Mutated Patients. *Cells*, 11.
- YIN, W., LIVRAGHI-BUTRICO, A., SEARS, P. R., ROGERS, T. D., BURNS, K. A., GRUBB, B. R. & OSTROWSKI, L. E. 2019. Mice with a Deletion of Rsph1 Exhibit a Low Level of Mucociliary Clearance and Develop a Primary Ciliary Dyskinesia Phenotype. *Am J Respir Cell Mol Biol*, 61, 312-321.
- ZABNER, J., KARP, P., SEILER, M., PHILLIPS, S. L., MITCHELL, C. J., SAAVEDRA, M., WELSH, M. & KLINGELHUTZ, A. J. 2003. Development of cystic fibrosis and noncystic fibrosis airway cell lines. *Am J Physiol Lung Cell Mol Physiol*, 284, L844-54.
- ZHU, X., LIU, Y. & YANG, P. 2017. Radial Spokes-A Snapshot of the Motility Regulation, Assembly, and Evolution of Cilia and Flagella. *Cold Spring Harb Perspect Biol,* 9.

Figures

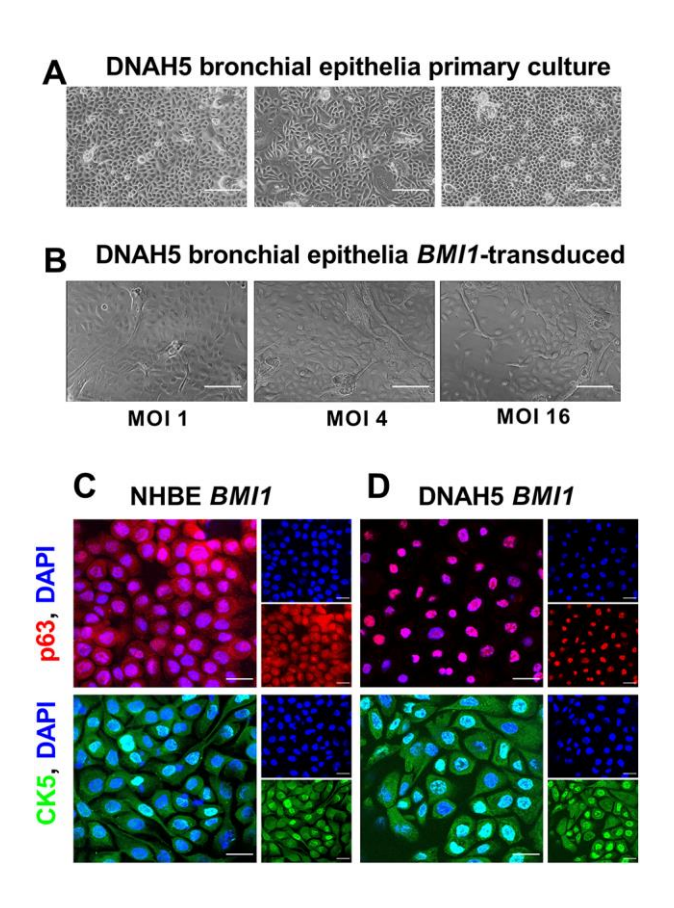
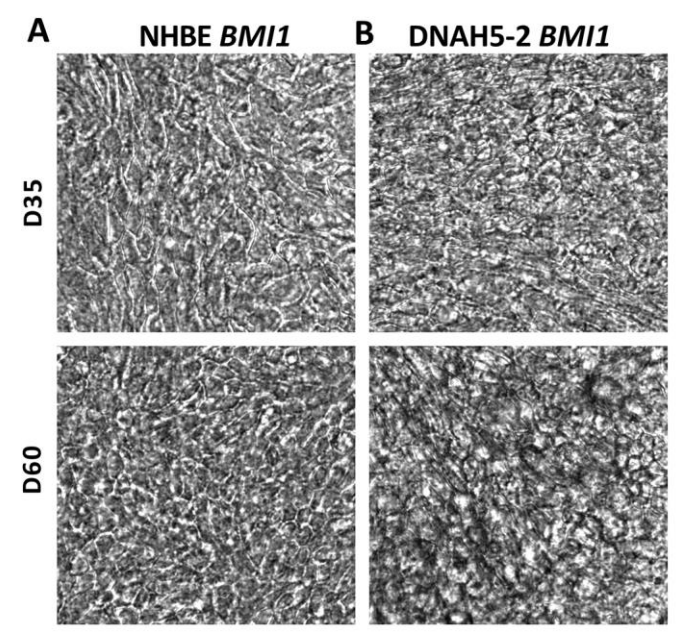
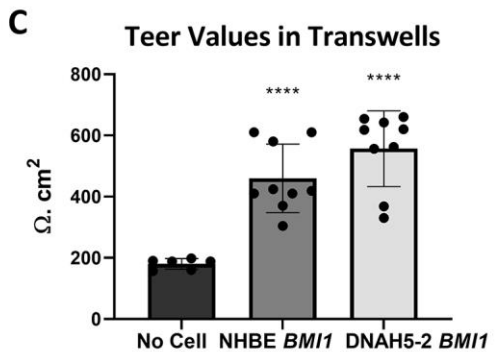


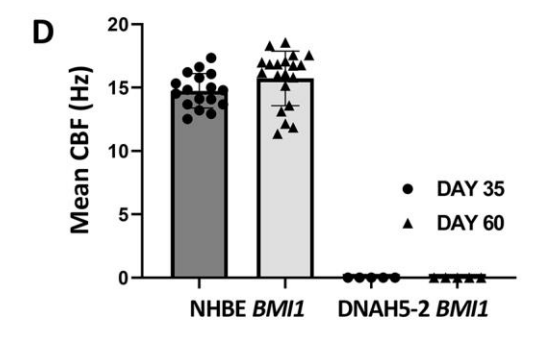
Fig. 1. Primary cell culture and lentiviral transduction of *DNAH5*-1 PCD bronchial epithelia

A) Primary bronchial airway epithelial cells from PCD patient DNAH5-1 at day 7 post seeding (3 different wells), scale bars represent 100 μm; **B)** DNAH5-1 cells after *BMI1* transduction (p2) at three different MOIs (1, 4, 16); **C, D)** Overlay of confocal images showing nuclear expression of p63 (red) and nuclear/cytoplasmic expression of CK5 (green) basal airway stem cell marker in *BMI1* -transduced NHBE cells (p2,9) (**C**) and in *BMI1*-transduced cells from PCD donor DNAH5-1 (p1,10) (**D**). DAPI (nuclei) in **C)** and **D)** were stained blue. Scale bars represent 20 μm.





High velocity video microscopy



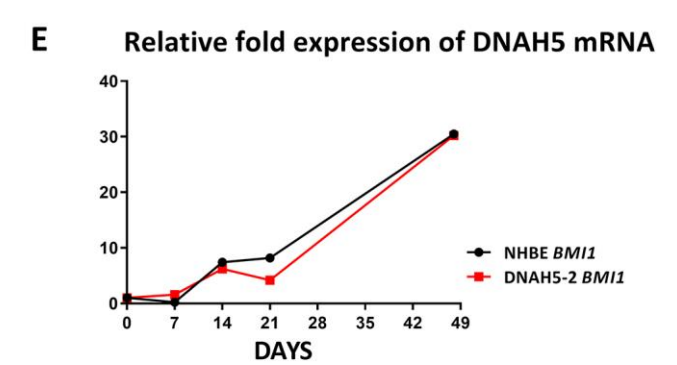


Fig. 2. Analysis of *BMI1* transduced *DNAH5-2* PCD airway epithelial cilia function

A. *BMI1* -transduced NHBE cells (p2,12) and **B.** *BMI1*-transduced basal cells from patient DNAH5-2 (p1,12) grown on transwell membranes at day 35 and day 60 of ALI cultures. **C.** Epithelial cell resistance of both NHBE and DNAH5-2 cells at D30 of ALI were similar, with no statistical significance (Mann-Whitney U test, p> 0.05, n=9). **D.** High velocity video microscopy recordings show 14.74 Hz and 15.72 Hz cilia beating frequency for NHBE cells at day 35 and day 60 respectively, indicating functional cilia motility, while DNAH5-2 cells display immotile cilia (n=17 and 20 fields of view for NHBE *BMI1* cells at D 35 and D60, n=5 fields of view for DNAH5-2 *BMI1* cells respectively). **E.** *DNAH5* mRNA expression in both NHBE and DNAH5 cells increased up to 30-fold over the course of 49 days of differentiation in ALI culture (n=3 per time point).

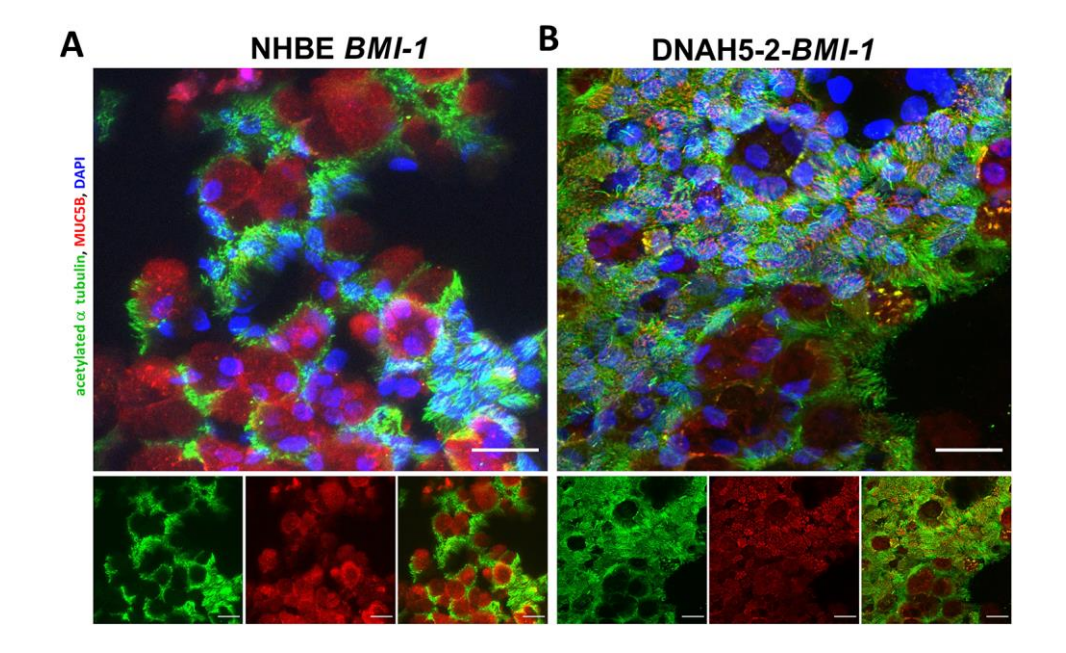


Fig. 3. Differentiation of *BMI1*-transduced *DNAH5-2* PCD airway progenitor cells

3D reconstruction of confocal images stained for acetylated α tubulin (green) MUC5B (red) and nucleus (DAPI in blue) showing differentiation of basal airway cells into ciliated, mucus-producing cells in day 30 of ALI. **A.** NHBE *BMI1* cells (p2,9) and **B.** DNAH5 *BMI1* cells from donor DNAH5-2 (p1,10). Scale bars represent 20 μ m.

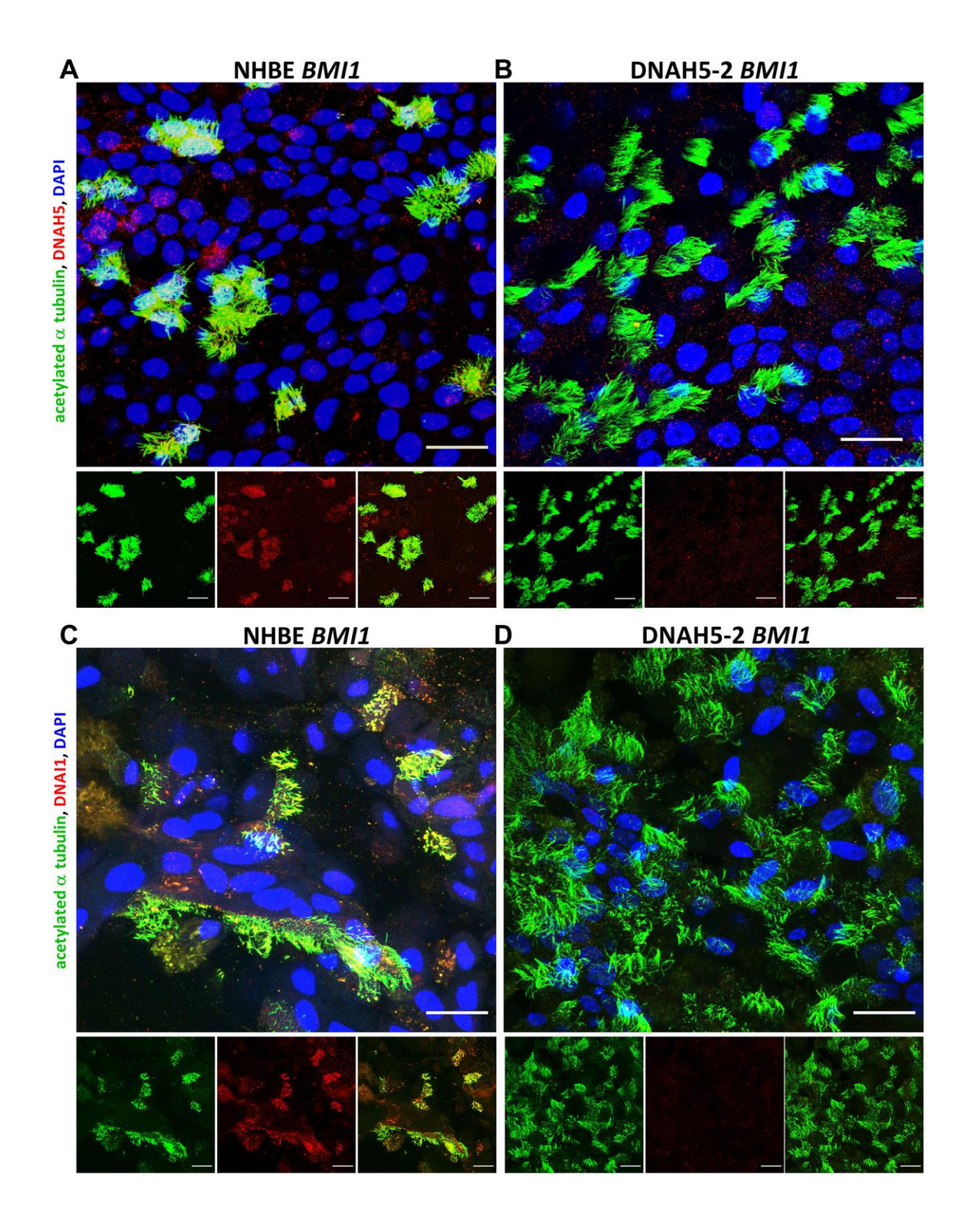


Fig. 4. Characterisation of DNAH5 and DNAI1 localisation in *BMI1*-transduced *DNAH5-2* PCD airway cell cilia

3D reconstruction of confocal images showing ciliary localisation of acetylated α -tubulin (green) and DNAH5/DNAI1(red) in differentiated airway epithelial cells with

DAPI (blue) staining of the nucleus. **A)** DNAH5 was present in cilia in NHBE *BMI1* cells (p2,9) but **B)** absent in the cilia of DNAH5 mutant *BMI1* cells (patient DNAH5-2; p1,10). **C)** DNAI1 was present in cilia in NHBE *BMI1* cells but **D)** absent in the cilia of DNAH5 mutant *BMI1* cells at day 30 of differentiation. Scale bars represent 20 μ m.

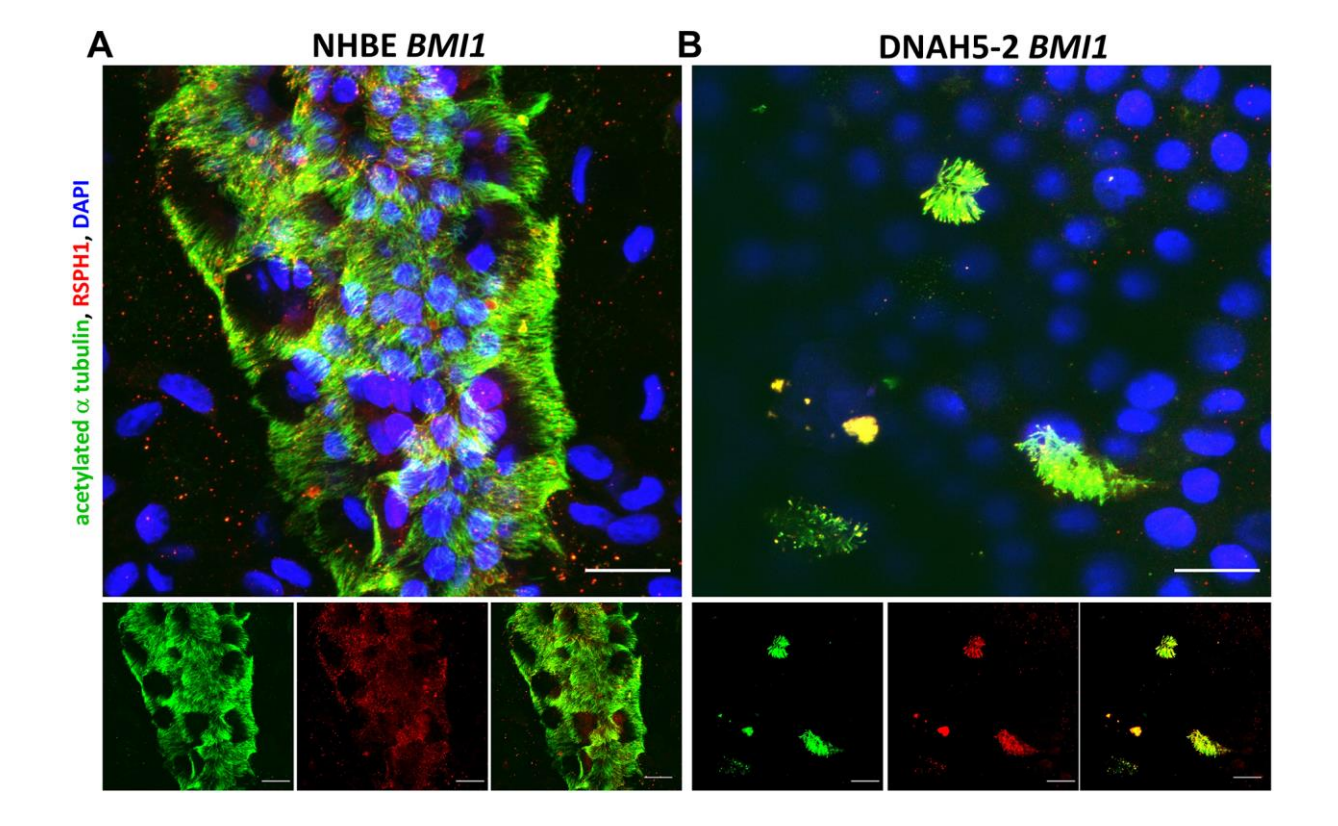


Fig. 5. Characterisation of RSPH1 localisation in *BMI1*-transduced *DNAH5*-2 PCD airway cell cilia

3D reconstruction of confocal images showing ciliary localisation of acetylated α tubulin (green) and RSPH1 (red) in differentiated airway epithelial cells with DAPI-stained nuclei (blue). **A)** RSPH1 was present in cilia in both NHBE *BMI1* cells and **B)** in the cilia of DNAH5-2-*BMI1* cells, at D30 of differentiation. Scale bars represent 20 μ m.

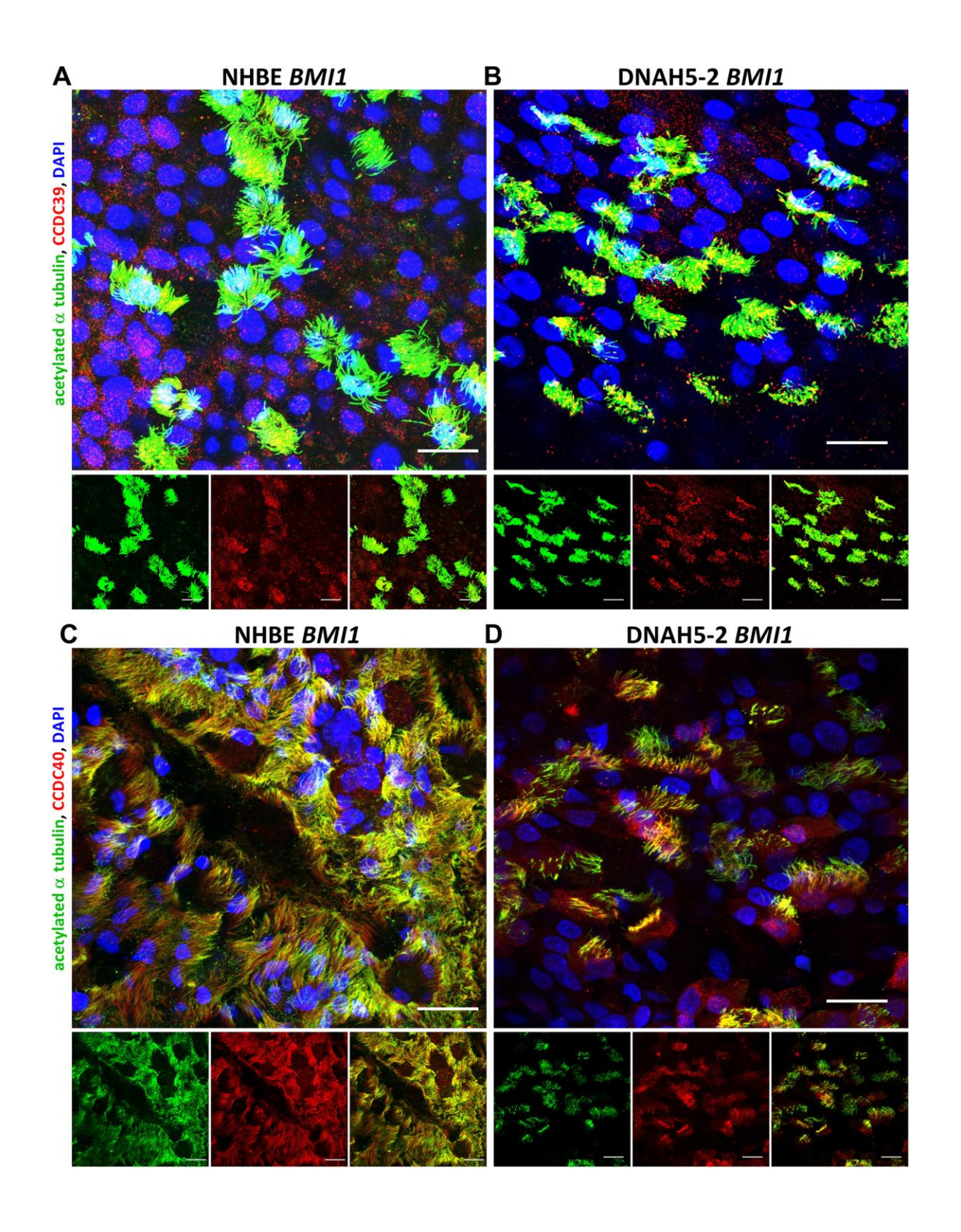


Fig. 6. Characterisation of CCDC39 and CCDC40 localisation in *BMI1*-transduced *DNAH5-2* PCD airway cell cilia

3D reconstruction of confocal images showing ciliary localisation of acetylated α tubulin (green) and CCDC39 (red) with DAPI-stained nuclei (blue) in differentiated

airway epithelial cells. **A)** CCDC39 was shown to be present in cilia of both NHBE *BMI1* cells (p2,9) and **B)** PCD cells from donor DNAH5-2; p1,10). CCDC40 was localised in cilia of both **C)** NHBE *BMI1* cells and **D)** in DNAH52-*BMI1* cells, at day 30 of differentiation. Scale bars represent 20 µm.

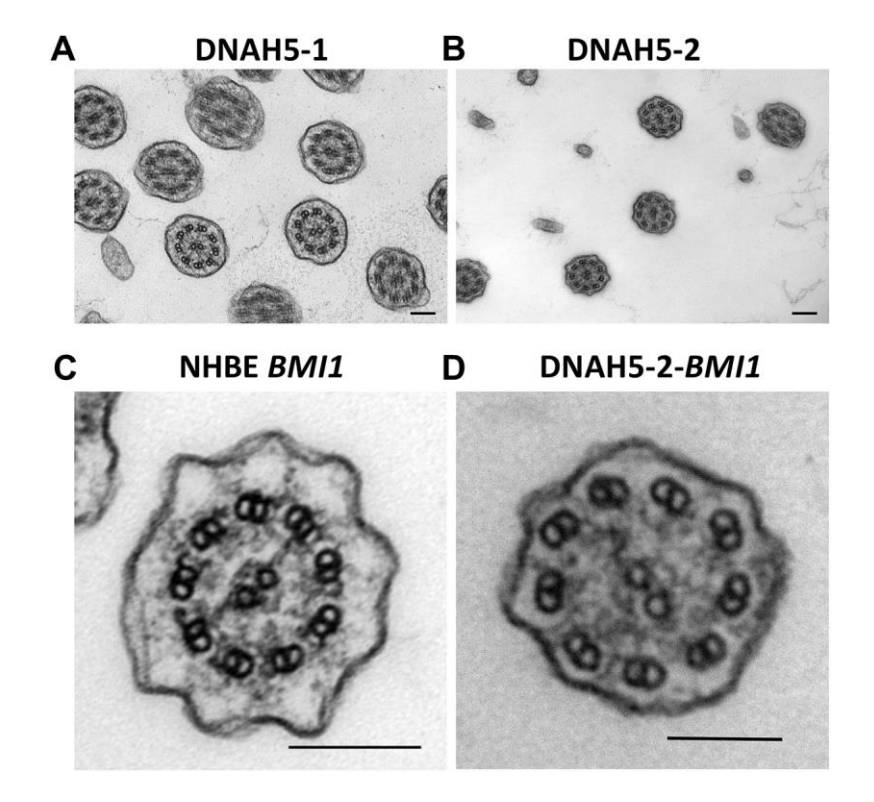


Fig. 7. TEM analysis of outer dynein arms in *BMI1* transduced DNAH5 variant PCD airway cilia transduced with *BMI1*

Cilia cross sections from, **A)** primary cells from donor DNAH5-1 before *BMI1* transduction (scale bar = 100 nm) **B)** primary cells from DNAH5-2 patient, before *BMI1* transduction (scale bar = 200 nm). TEM images show missing inner and outer dynein arms (IDA/ODA). **C)** NHBE *BMI1*-transduced cells with IDA and ODA present and **D)** *BMI1*-transduced DNAH5-2 donor cells showing cilia with missing IDA and ODA. Scale bars represent 100 nm.

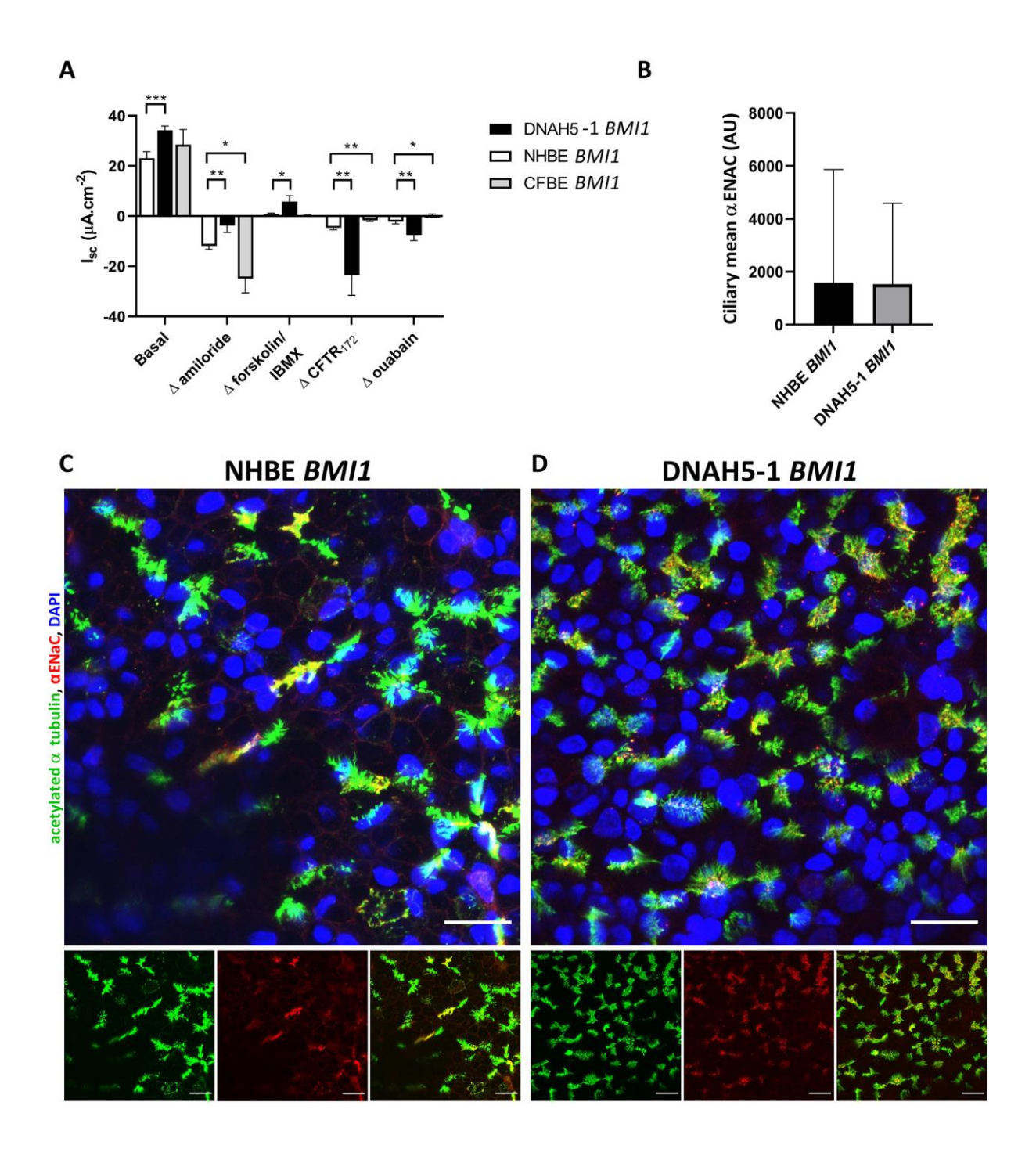


Fig. 8. Characterisation of ion transport in *BMI1*-transduced DNAH5-1 PCD airway cells and ciliary ENaC localisation

A) Spontaneous (Basal) mean short circuit current (I_{sc}) or change in I_{sc} (ΔI_{sc}) in response to drugs inhibiting ENaC (Δ amiloride), activating CFTR (Δ forskolin/IBMX), inhibiting CFTR activity (Δ CFTR₁₇₂) or inhibiting Na+/K+-ATPase (Δ ouabain) of NHBE *BMI1* cells, DNAH5-1 *BMI-1* cells (DNAH5-1, bronchial origin) and CFBE *BMI1* cells at Day 30 of ALI culture. Inhibitory ΔI_{sc} are shown as negative changes

and stimulatory ΔI_{sc} are shown as positive changes. (n =3, *p< 0.05, **p < 0.01, ***p < 0.001, Mann-Whitney U test). **B)** Mean ciliary $\alpha ENaC$ of NHBE *BMI1* and DNAH5-1 *BMI1* cells from 3D reconstruction of confocal images of ALI cultures at D30, quantified by IMARIS software, n \geq 5 fields of view, >10000 ciliary measurement per sample. **C)** 3D reconstruction of confocal images showing ciliary localisation of acetylated α tubulin (green) and $\alpha ENaC$ (red) in differentiated bronchial epithelial cells (NHBE-*BMI1* cells, p2,17) and in **D)** differentiated DNAH5-1 *BMI1* patient airway cells at 30 days of differentiation (p1,18), DAPI-stained nuclei (blue), scale bars represent 20 µm.

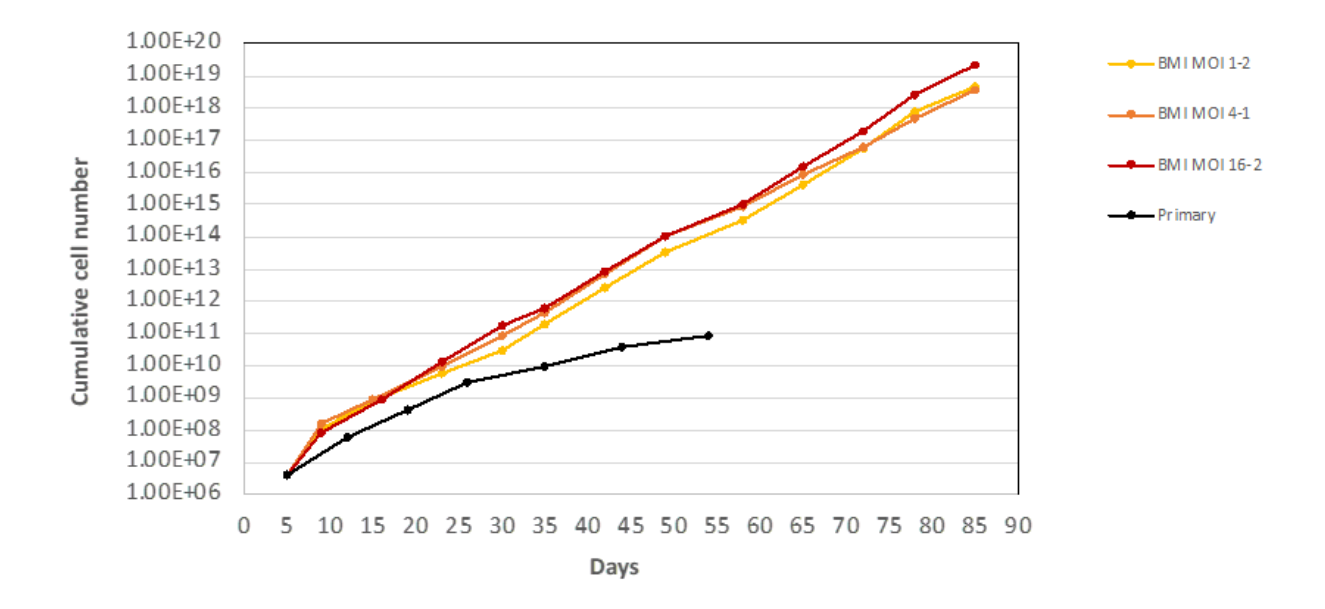


Fig. S1. Growth curve of *BMI1* transduced normal human bronchial epithelial (NHBE) cells Primary NHBE cells were transduced with *BMI1* lentivirus at three MOIs (I, 4 and 16) and were cultured up to 90 days. Growth curves were generated compared to non-transduced primary cells.

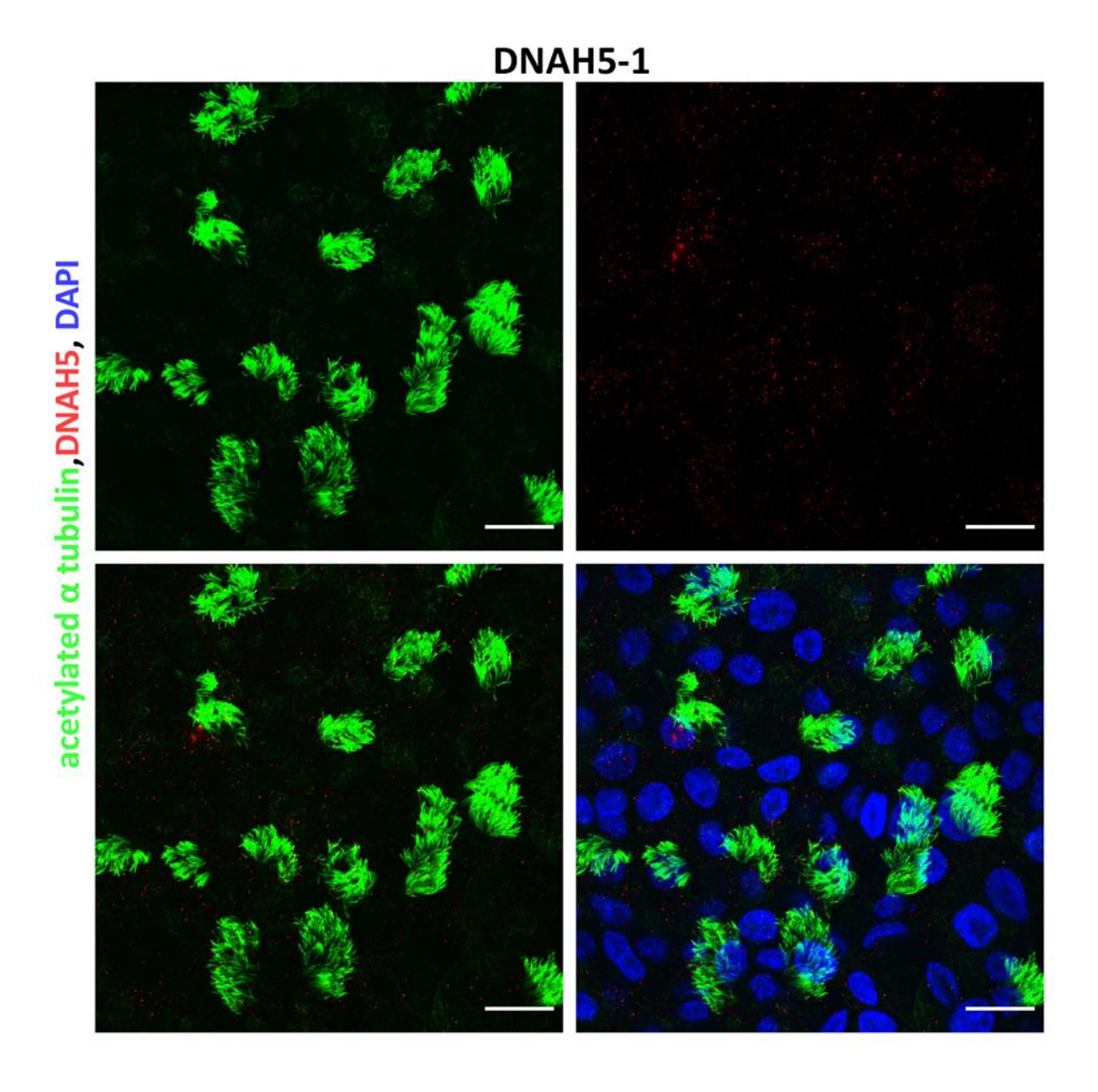


Fig. S2. Characterisation of DNAH5 localisation in *BMI1*-transduced *DNAH5-1* PCD bronchial airway cell cilia

3D reconstruction of confocal images showing ciliary localisation of acetylated α -tubulin (green) and the absence of DNAH5 (red) in differentiated DNAH5-1 *BMI1* cells of bronchial origin (patient DNAH5-1; p1,10) at day 30 of differentiation. Overlay of both and all channels in bottom panel, DAPI in blue Scale bars represent 20 μ m.

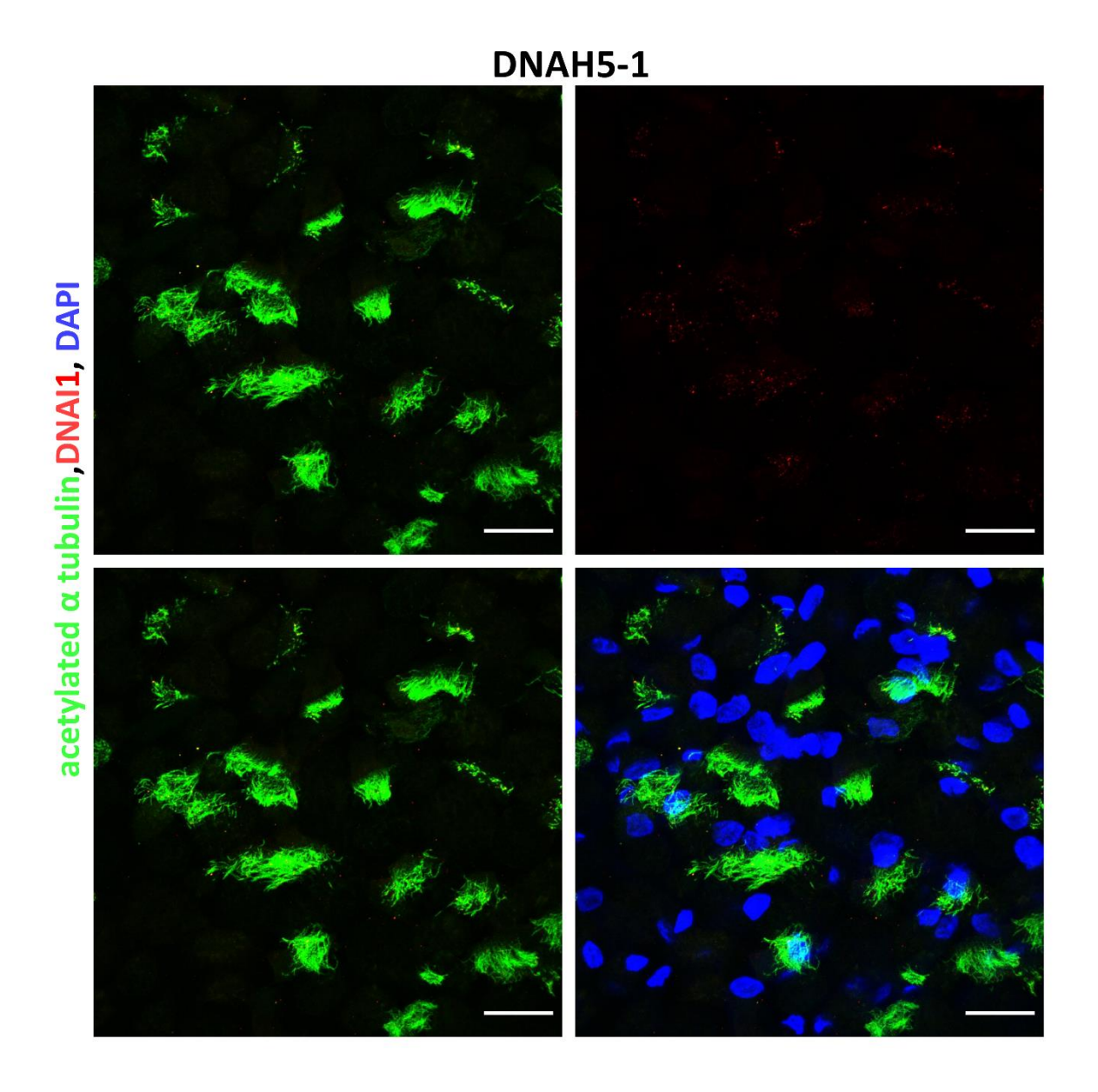


Fig. S3. Characterisation of DNAI1 localisation in *BMI1*-transduced *DNAH5-1* PCD bronchial airway cell cilia

3D reconstruction of confocal images showing ciliary localisation of acetylated α -tubulin (green) and the absence of DNAI1 (red) in differentiated DNAH5-1 *BMI1* cells of bronchial origin (patient DNAH5-1; p1,10) at day 30 of differentiation. Overlay of both and all channels in bottom panel, DAPI in blue Scale bars represent 20 μ m.

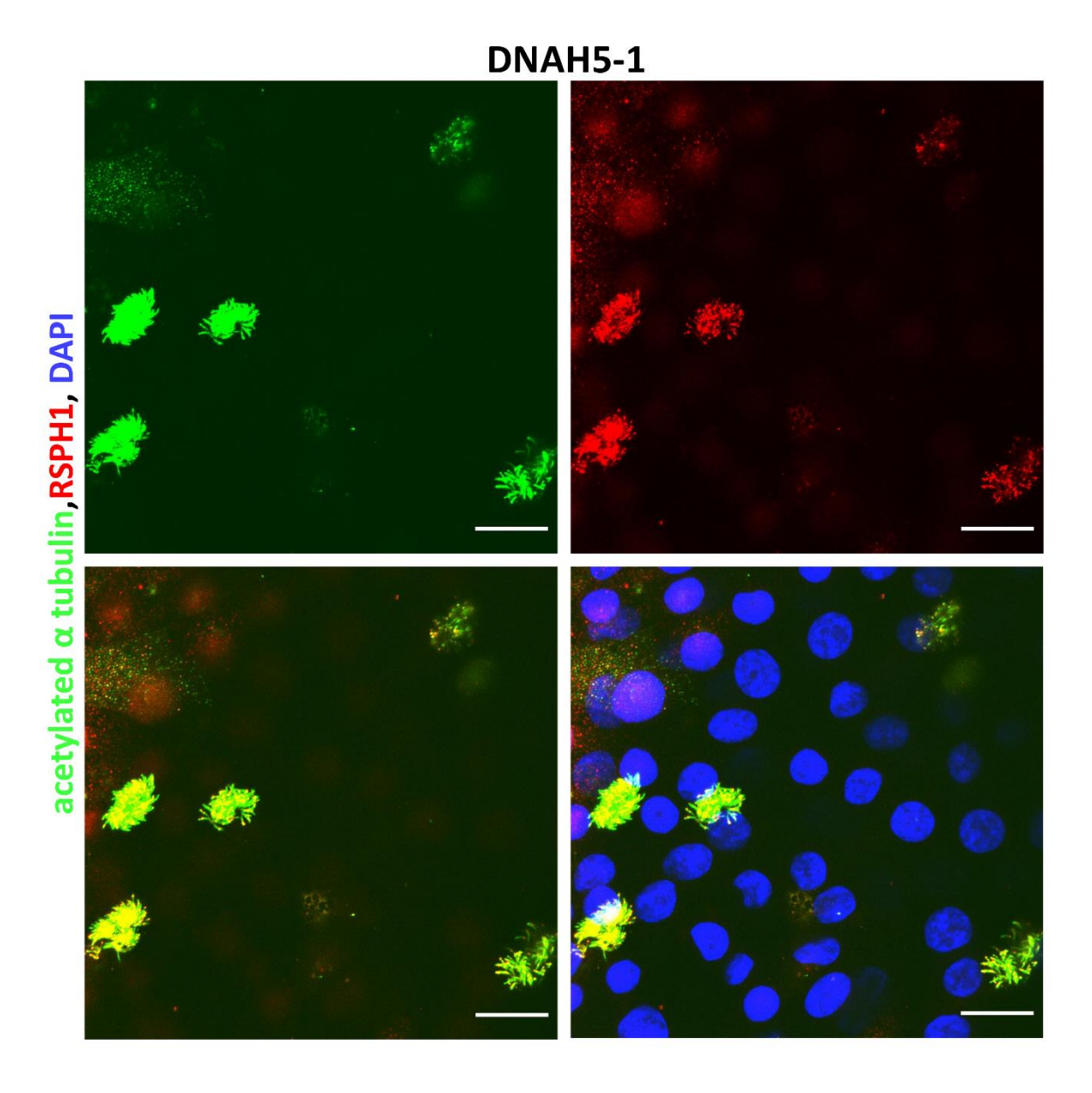


Fig. S4. Characterisation of RSPH1 localisation in *BMI1*-transduced *DNAH5-1* PCD bronchial airway cell cilia

3D reconstruction of confocal images showing ciliary localisation of acetylated α -tubulin (green) and RSPH1(red) in differentiated DNAH5-1 *BMI1* cells of bronchial origin (patient DNAH5-1; p1,10) at day 30 of differentiation. Overlay of both and all channels in bottom panel, DAPI in blue Scale bars represent 20 μ m.

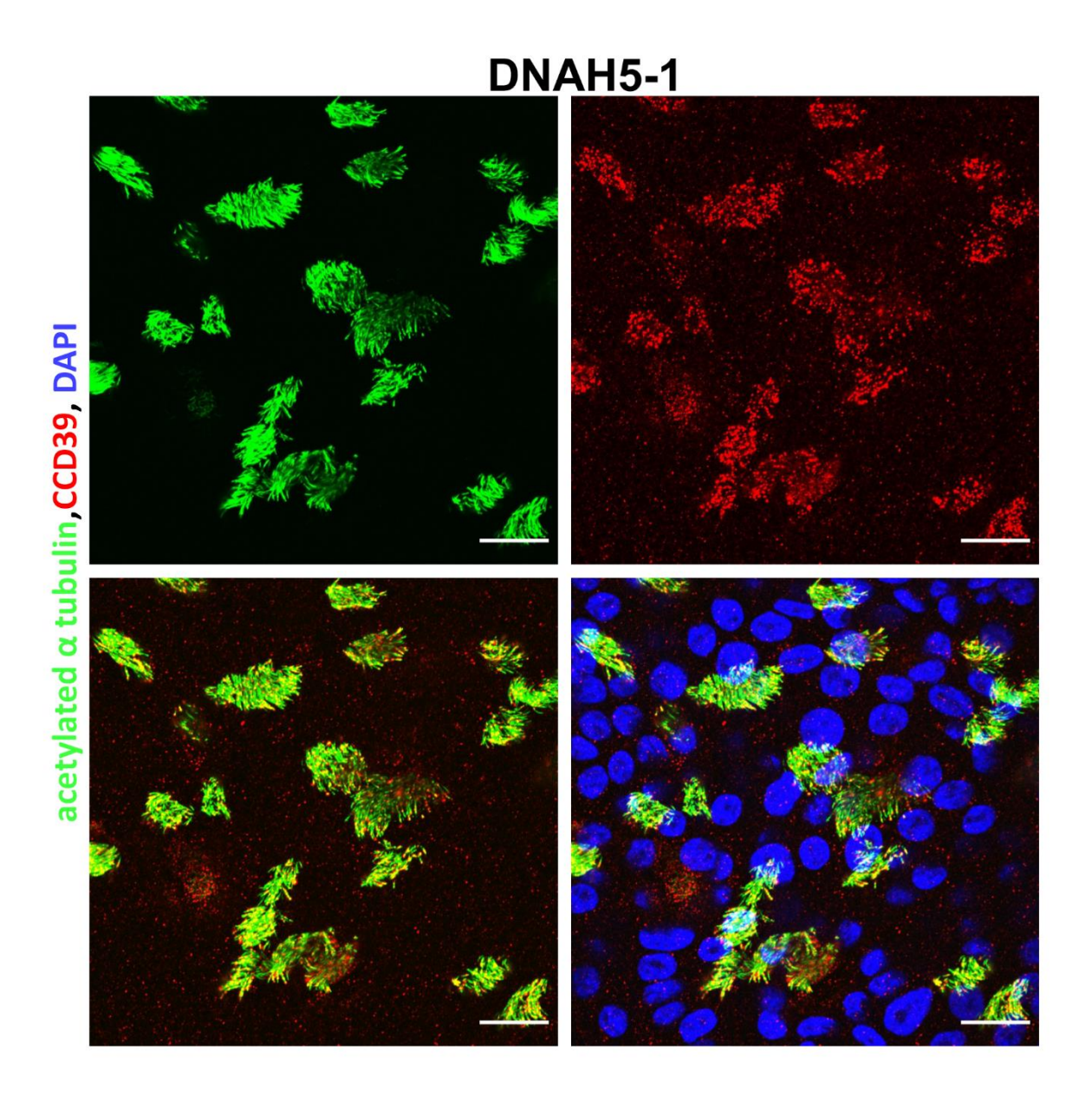


Fig. S5. Characterisation of CCD39 localisation in *BMI1*-transduced *DNAH5-1* PCD bronchial airway cell cilia

3D reconstruction of confocal images showing ciliary localisation of acetylated α -tubulin (green) and CCD39 (red) in differentiated DNAH5-1 *BMI1* cells of bronchial origin (patient DNAH5-1; p1,10) at day 30 of differentiation. Overlay of both and all channels in bottom panel, DAPI in blue Scale bars represent 20 μ m.

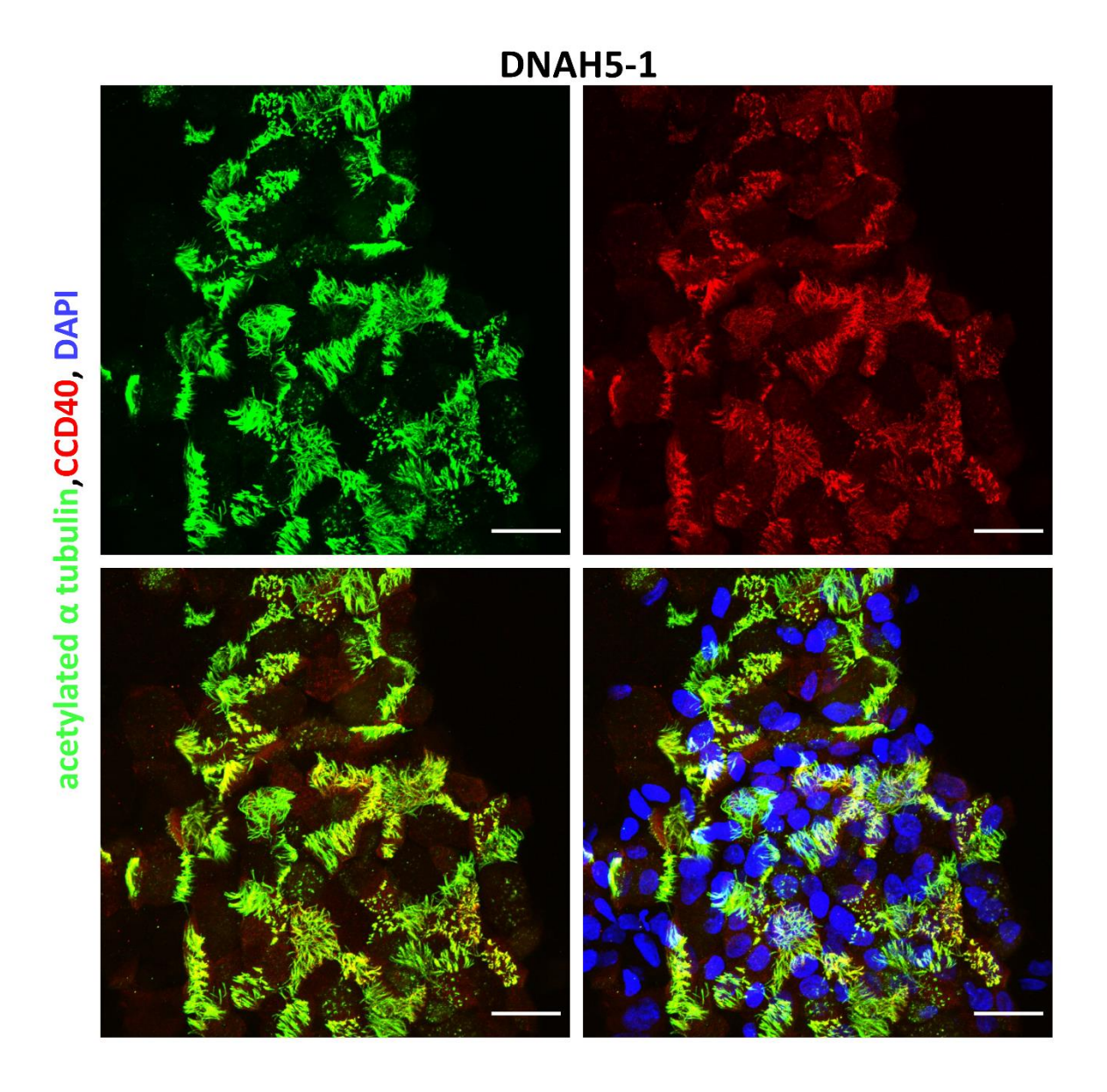


Fig. S6. Characterisation of CCD40 localisation in *BMI1*-transduced *DNAH5-1* PCD bronchial airway cell cilia

3D reconstruction of confocal images showing ciliary localisation of acetylated α -tubulin (green) and CCD40 (red) in differentiated DNAH5-1 BMI1 cells of bronchial origin (patient DNAH5-1; p1,10) at day 30 of differentiation. Overlay of both and all channels in bottom panel, DAPI in blue Scale bars represent 20 μm .

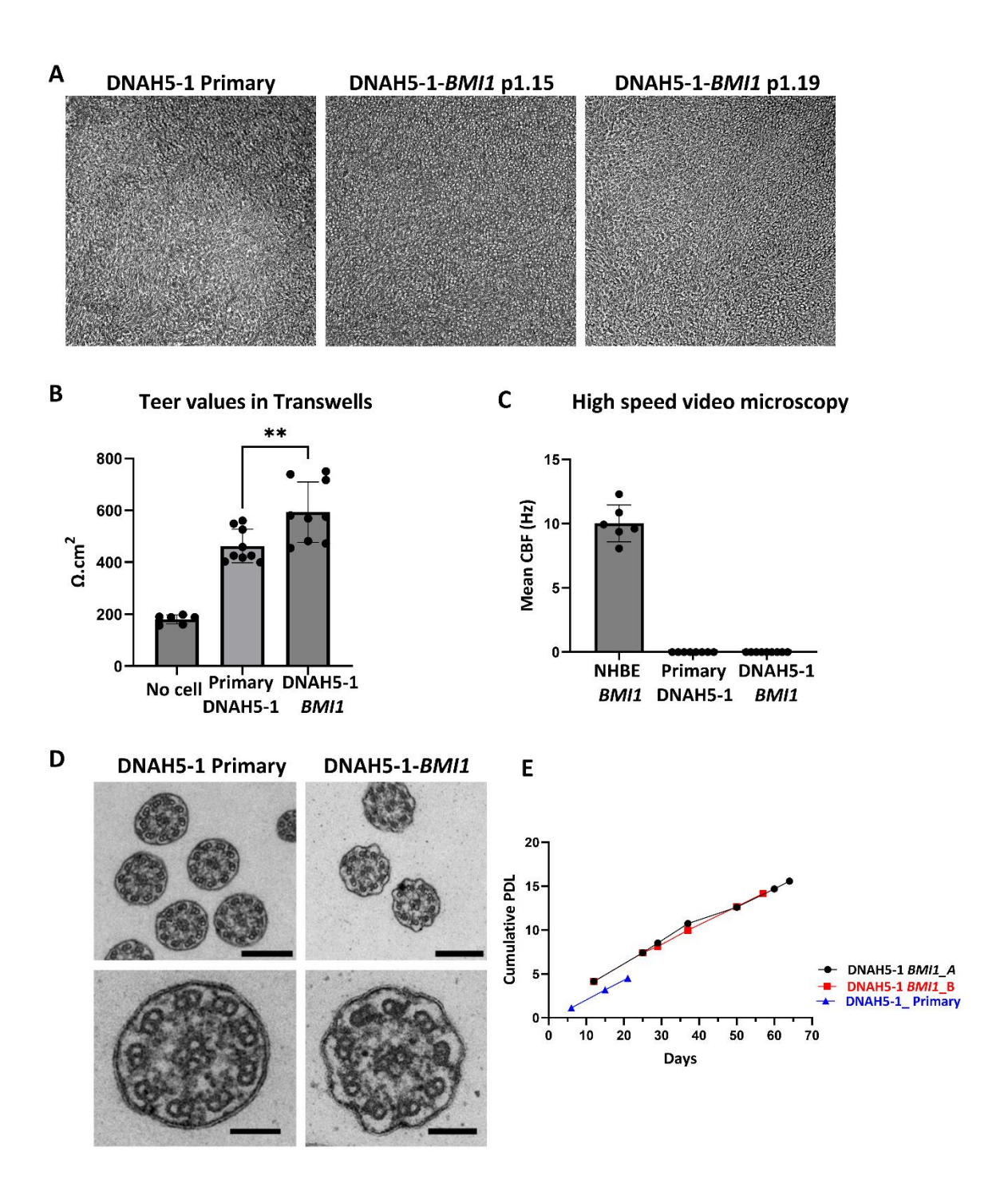


Fig. S7. Analysis of primary DNAH5-1 vs late passage *BMI1* transduced DNAH5-1 airway epithelial cell characteristics.

A. Primary DNAH5-1 cells (p3) and *BMI1*-transduced DNAH5-1 cells (p1,15 and p1,19) grown on transwell membranes at day 60 of ALI cultures. **B**. Epithelial cell resistance of *BMI1*-transduced DNAH5-1 cells (p1,19) were higher than the non-transduced primary DNAH5-1 cells at day 60 of ALI (Mann-Whitney U test, p> 0.01, n=9). **C**. High speed video microscopy recordings show a mean of 10 Hz cilia beating frequency for NHBE cells (p2,13) at day 60 of ALI, indicating functional cilia motility,

while both primary (p3) and *BMI1*-transduced DNAH5-1 cells (p1,19) display immotile cilia ($n \ge 6$ fields of view). **D.** TEM analysis of cilia cross section of primary cells from donor DNAH5-1 before *BMI1* transduction (p3) on the left and after *BMI1* transduction (p1,19) on the right, showing missing ODA in both. Scale bars represent 250 nM for the top panel and 100 nM for the lower panel **E.** Growth curve of primary vs *BMI1* transduced DNAH5-1 cells cultured from p1,8 (DNAH5-1 *BMI1*_A) and from p1,12 (DNAH5-1 *BMI1*_B) up to 60 days in culture vs primary DNAH5-1 cells without *BMI1* transduction that stopped growing after p5.

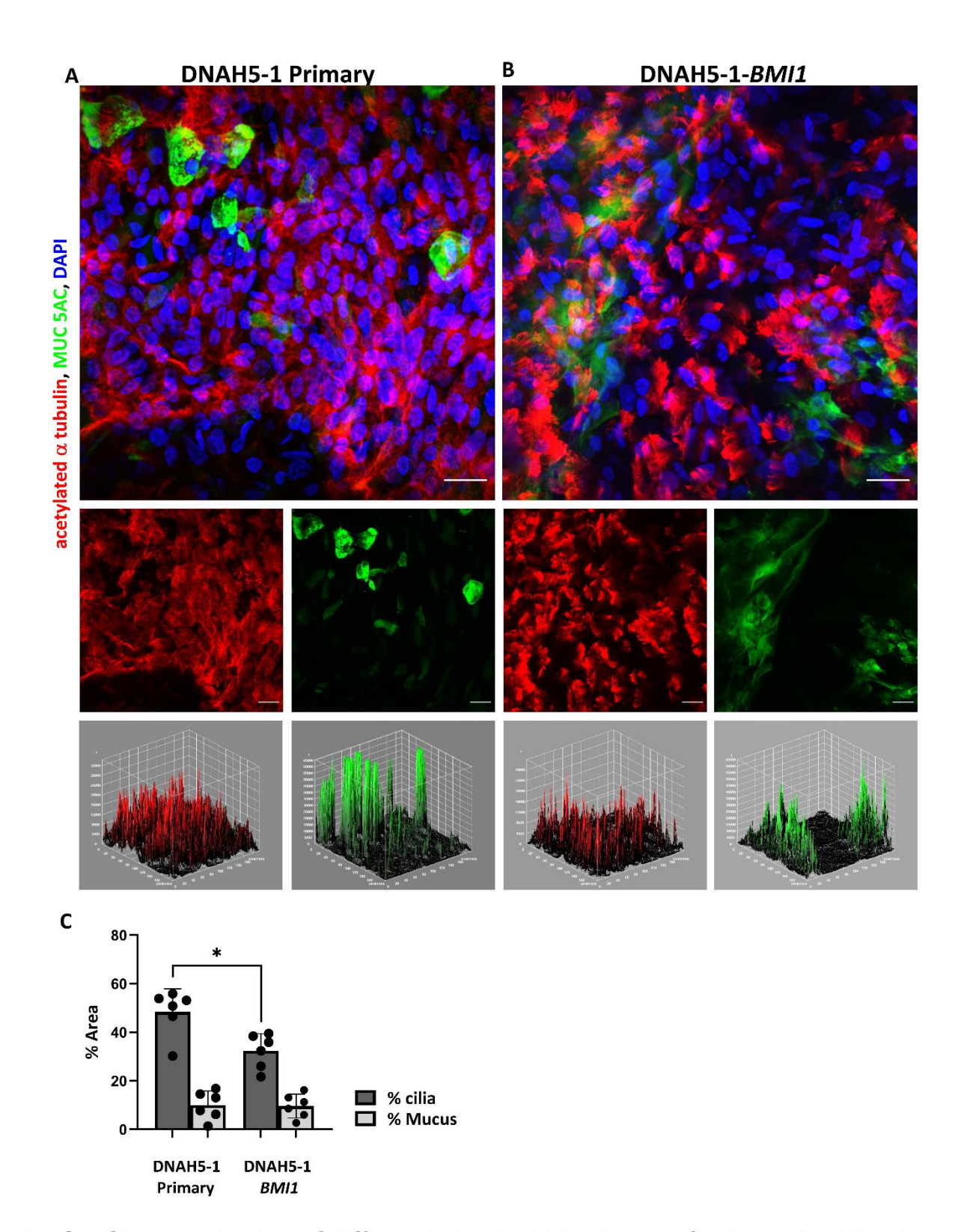


Fig. S8. Characterisation of differentiation in ALI cultures of primary DNAH5-1 cells and *BMI1* transduced DNAH5-1 cells

3D reconstruction of confocal images stained for acetylated α tubulin (red), MUC5AC (green) and nucleus (DAPI in blue) showing differentiation of basal airway cells into ciliated, mucus-producing cells at day 60 of ALIA. Primary DNAH5-1 cells before transduction (p3) and **B.** DNAH5 *BMI1* cells from donor DNAH5-1 (p1,19). Scale bars represent 20 μ m. **C**. Quantification of cilia % area and MUC5AC % area in both primary DNAH5-1 and DNAH5-1 *BMI1* airway epithelial cells in ALI culture at Day 60 of differentiation from 3D reconstruction of confocal images, (n=6 fields per group,*p < 0.05, Mann-Whitney U test).

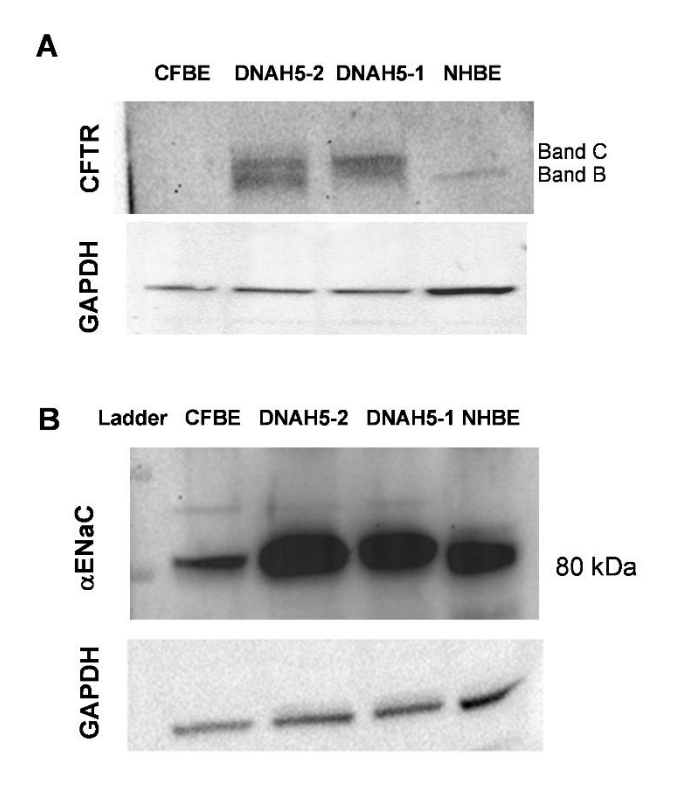


Fig. S9. Immunoblotting for $\alpha ENaC$ and CFTR.

Protein samples from PCD-*BMI1* epithelial cells (DNAH5-1 and DNAH5-2), CF-*BMI1* bronchial epithelial cells (CFBE) and normal human bronchial epithelial cells-*BMI1* (NHBE) were analysed by electrophoretic separation and immunoblotting for CFTR (A) and α ENaC (B). A) The double bands for CFTR are characteristic of the lower molecular weight, core glycosylated protein (B form) and the slower migrating, complex glycosylated protein (C form). B) α ENaC staining reveals the ~80 kDa protein. To ensure similar levels of protein, samples were also stained for the housekeeping gene, GAPDH.

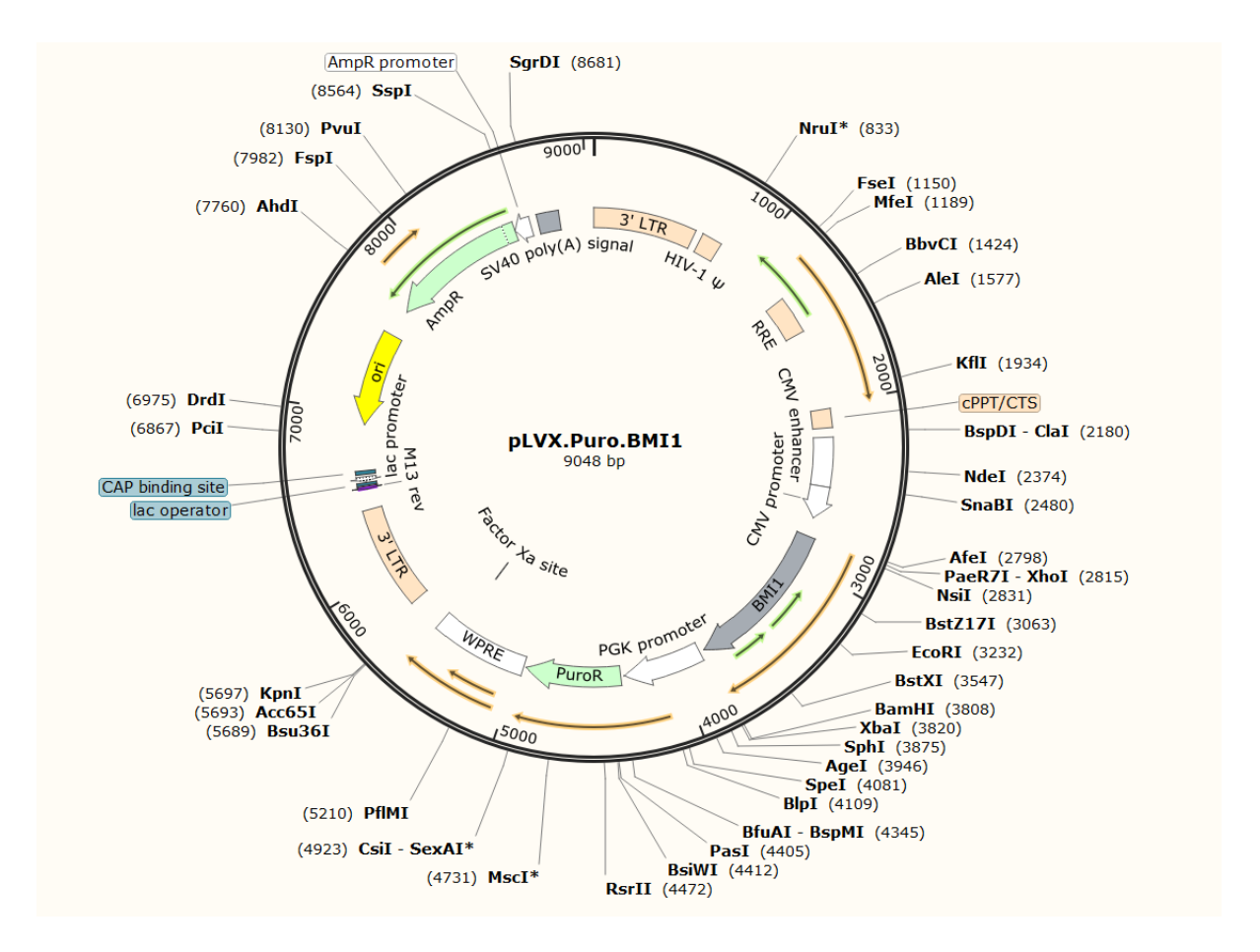


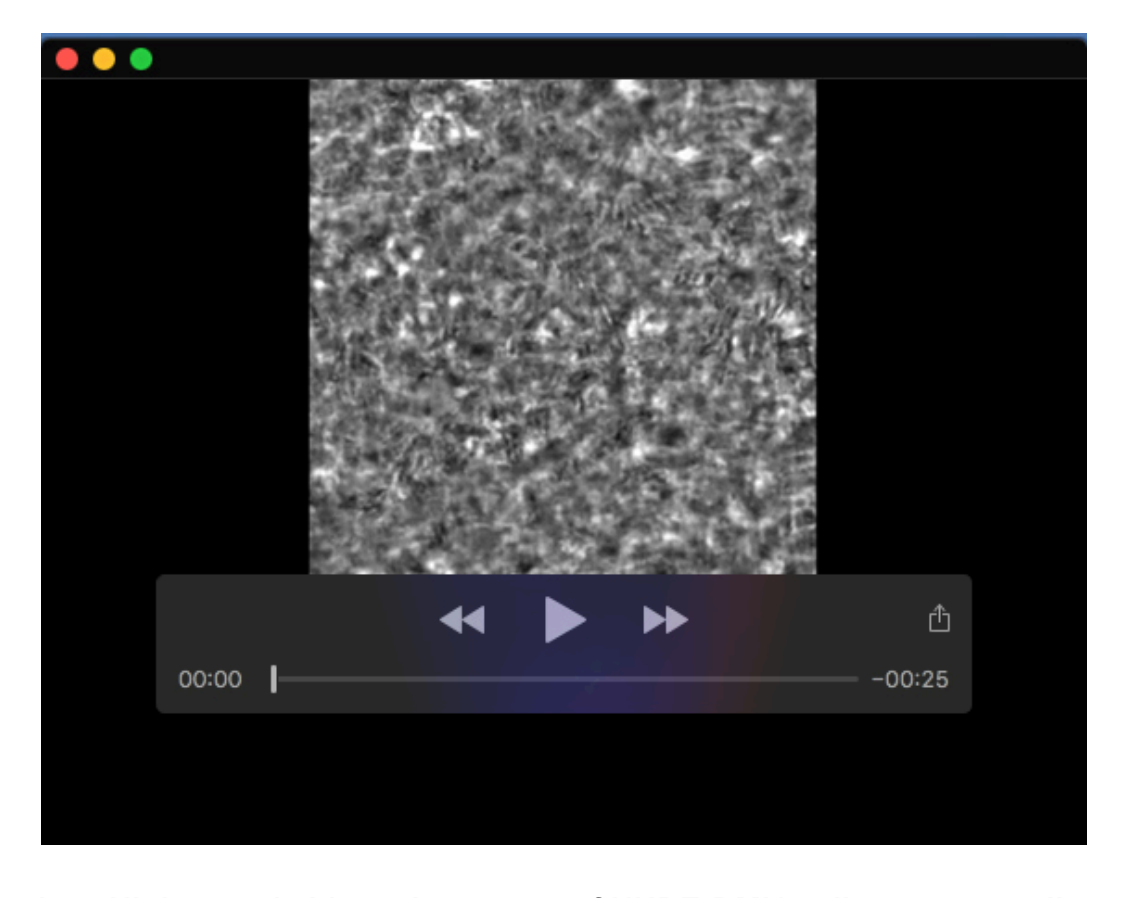
Fig. S10. pLVX.Puro.BMI1 plasmid map

Table S1. DNAH5 variants from PCD donors

Donor	Age at sampling	Sex	Allele 1 cDNA, protein	Allele 1 dbSNP protein	Allele 2 cDNA, protein	Allele 2 dbSNP protein	Tissue source
DNAH5-1	4 years old	М	c.10825C>T;_p.(Gln3609Ter)	rs749980719	c.3466del; p.(lle1156fs)	rs775866092	Bronchoscopy
DNAH5-2	8 years old	М	c.13458dup; p.(Asn4487Ter)	rs775696136	c.13486C>T; p.(Arg4496Ter)	rs200901816	Nasal brushing



Movie 1. High speed video microscopy of NHBE-BMI1 cells on transwells at day 35 of ALI culture displaying motile cilia.



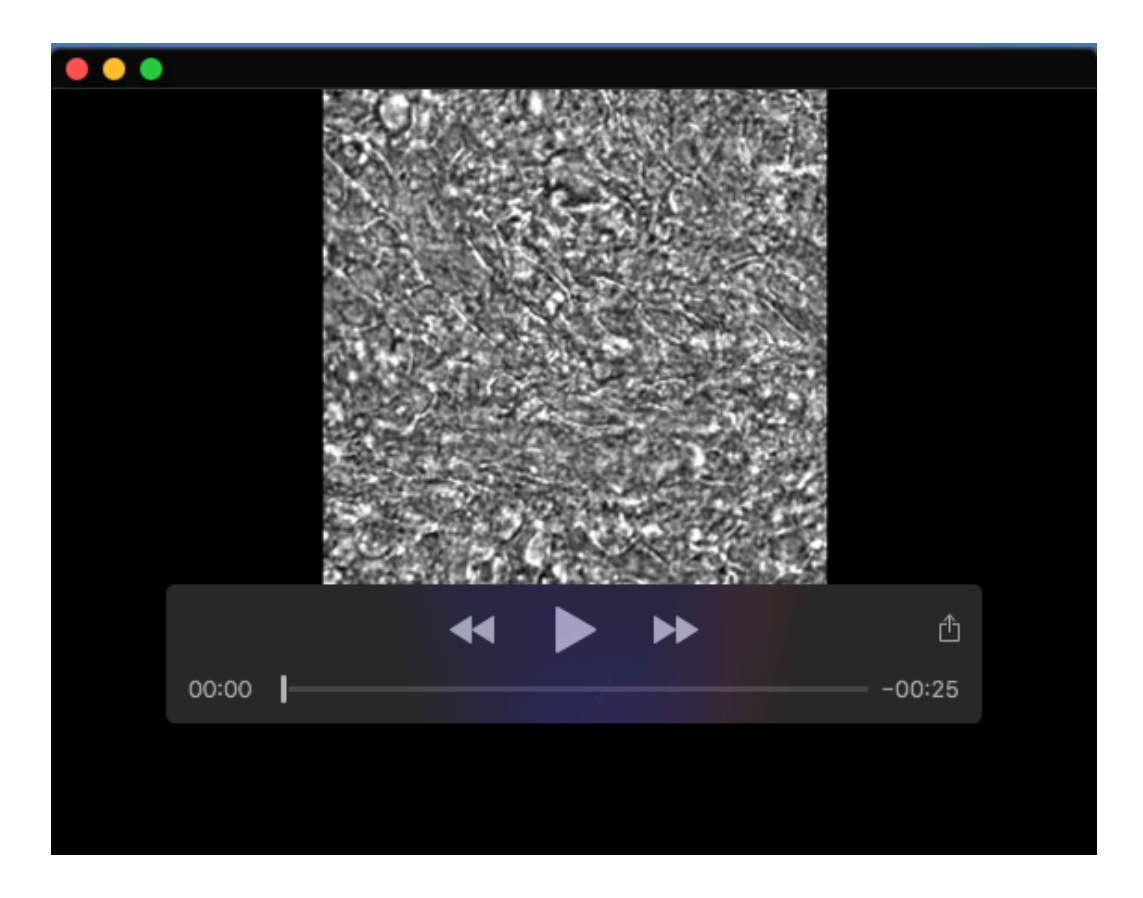
Movie 2. High speed video microscopy of NHBE-BMI1 cells on transwells at day 60 of ALI culture displaying motile cilia.



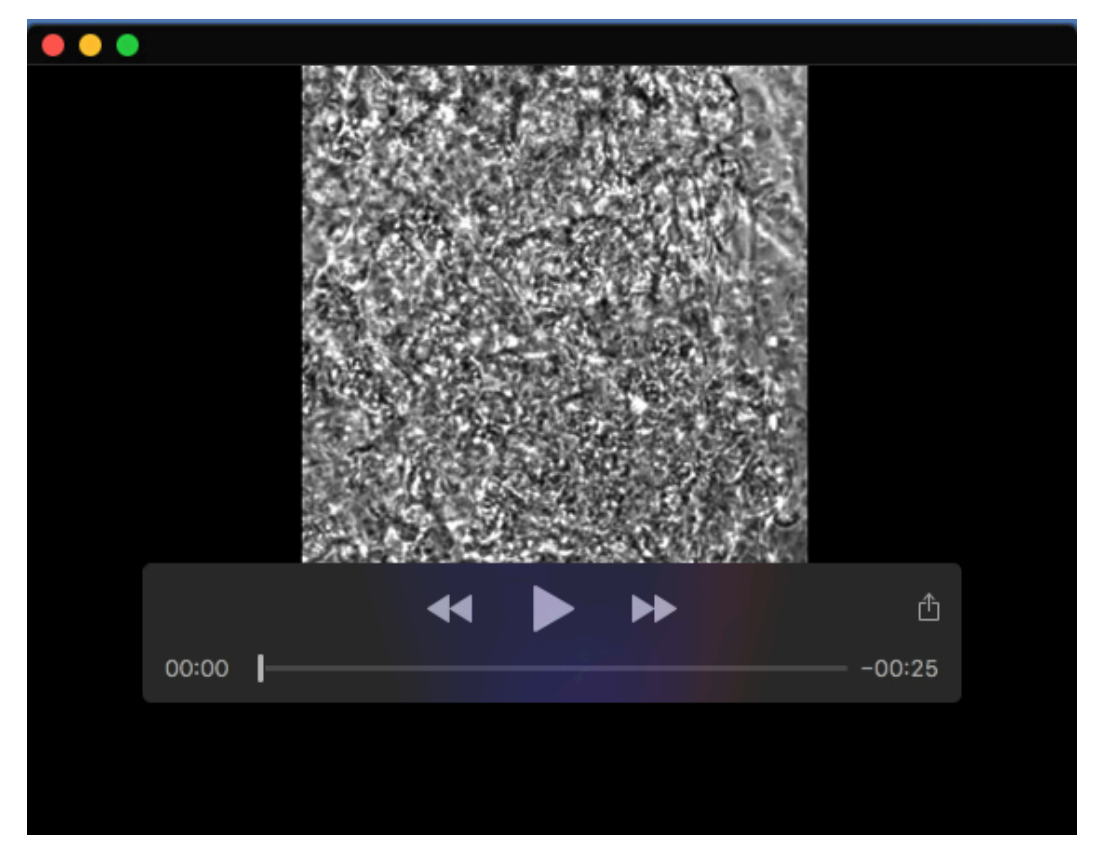
Movie 3. Light microscopy recordings of NHBE-BMI1 cells on a slide at day 60 of ALI culture displaying motile cilia from top view.



Movie 4. Light microscopy recordings of NHBE-BMI1 cells on a slide at day 60 of ALI culture displaying motile cilia from side view.



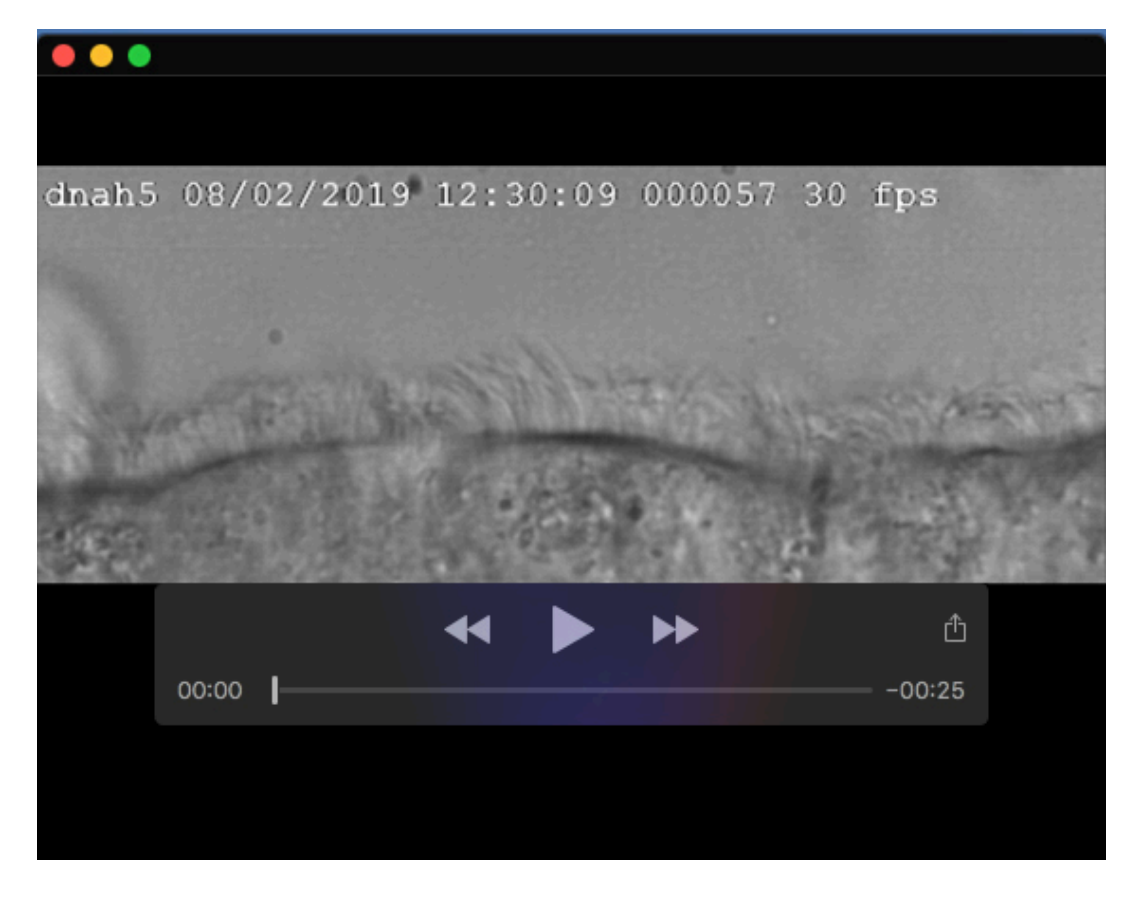
Movie 5. High speed video microscopy of DNAH5-2 -BMI1 cells on transwells at day 35 of ALI culture displaying immotile cilia.



Movie 6. High speed video microscopy of DNAH5-2 -BMI1 cells on transwells at day 60 of ALI culture displaying immotile cilia.



Movie 7. Light microscopy recordings of DNAH5-2-BMI1 cells on a slide at day 60 of ALI culture displaying mostly static cilia from top view.



Movie 8. Light microscopy recordings of DNAH5-2-*BMI1* cells on a slide at day 60 of ALI culture displaying mostly static cilia from side view.